If BNCs can be specifically delivered to brain tumors, they might be promising carriers of anti-tumor drugs to brain tumors and be effective for the treatment of brain tumors. The major component of BNC is the longest form of the envelope protein (L protein) and contains the preS1 region [74]. This region is the determinant of specific infectivity in human hepatocytes for BNC as well as HBV. Since it does not contain a viral genome, BNC is nontoxic to cells *in vitro* and safe *in vivo* especially to humans when used as vaccines. BNC is now being developed as a novel drug delivery vector capable of the specific delivery of genes, proteins and pharmaceutical drugs to human hepatocytes with high efficacy. When the pre-S1 region is replaced with other targeting moieties or biorecognition molecules, such as antibodies, receptors, and ligands, the specificity of BNC can be altered and may be applicable for the retargeting of BNCs to specific cells or tissues other than liver tissue [75].

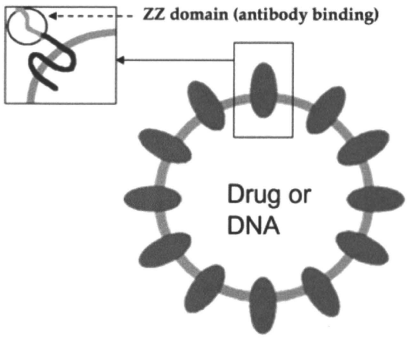

Fig. (3). Illustration of Bionanocapsules (ZZ-BNC).

To extend the targeting range of BNCs, the pre-S1 peptide on the surface of BNCs was replaced with the antibody affinity motif of protein A (ZZ), resulting in ZZ-BNC (Fig. **3**). ZZ-BNC bound with anti-human EGFR antibody was specifically delivered to cultured glioblastoma Gli36 cells overexpressing EGFR but not normal glial cells. The targeting of glioma was also confirmed in a mouse brain tumor model [76]. The fluospheres could be specifically delivered to Gli36 cells by the active targeting of zz-BNCs with anti-EGFR antibodies.

3.4. Multifunctional Nanoparticles

Multi-functionality provides advantages to nanoparticle-based DDS for the cancer-specific delivery of therapeutic or imaging agents. A universal nanoparticle-based platform can simultaneously detect, image, and deliver therapeutic compounds to tumor cells.

Tumor-specific accumulation of nanoparticles provides not only the means for drug delivery to the tumor, but also an opportunity to further conjugate a metallic core or shell for optical imaging or MRI in tumor diagnostics, guided hyperthermia therapy, and guided radiation therapy [77]. The use of targeted multifunctional nanoparticles can combine diagnosis with the treatment of brain tumors, such as the encapsulation of photodynamic therapy (PDT) agents (Photofrin®) with imaging agents (iron oxide) in polymeric nanoparticles. PDT involves the delivery of photosensitizers such as Photofrin® to tumors, combined with local excitation by the appropriate wavelength of light, resulting in the production of singlet oxygen and other reactive oxygen species. These initiate apoptosis and cytotoxicity in many types of tumors, with minimal systemic toxicity. PDT is more selective and less toxic than chemotherapy because the drug is not activated until the light is delivered. Reddy *et al.* linked a vascular-targeting peptide on the surface of nanoparticles encapsulated with photosensitizers and iron oxide. Significant MRI contrast enhancement was observed in glioma-bearing rats following intravenous administration. The survival rate in PDT-treated mice was also improved compared with controls [78].

For *in vitro* and *in vivo* optical imaging, semiconductor quantum dots (QDs) have recently emerged as a promising alternative to fluorescent markers; their superior brightness and photostability make them excellent candidates in the development of trackable multifunctional agents. Peptides (RGD) and antibodies have been conjugated to QDs for targeting in living subjects. Weng *et al.* constructed QD-conjugated immunoliposome-based nanoparticles (QD-ILs) with anti-HER2 scFv. Localization of QD-ILs at tumor sites was visualized by *in vivo* fluorescence imaging in nude mice bearing MCF-7/HER2 xenografts. Doxorubicin-loaded QD-ILs also showed efficient anticancer activity [79].

Mulder *et al.* used QDs conjugated to paramagnetic and pegylated lipids for combined fluorescence and MRI [80]. The specificity and sensitivity of the bimodal nanoparticles covalently linking RGD peptides were assessed and confirmed in cultured endothelial cells. Potentially, such nano-DDS could be used for the diagnosis of brain tumors with enhanced MRI imaging, and fluorescence emission from QDs could help physicians perform real-time tumor resection using optical guidance with encapsulated drug molecules providing post-surgical adjuvant therapy. Thus, drug molecules conjugated to these heterogeneous nanoparticles can provide additional functionalities. However, a disadvantage of QDs and metallic nanoparticles is known to be less biocompatible. For example, breakdown of semiconductor QDs composed of heavy metal ions could result in release of potent heavy metal ions such as cadmium ions and cause significant hepatotoxic effect in liver cells [81]. Compared with liposomes and polymers, there are many years away for QDs from reaching clinical trials.

The complexity of brain tumors also provides a challenge to constructing more effective multifunctional nanoparticles. Targeting brain tumors more accurately is the most important step. Till now, tumor surface markers used for targeted delivery include: EGFR; transferrin receptor; folate receptor; integrin $\alpha v\beta 3$; extracellular matrix (ECM) glycoproteins [82]. The targeting molecules for the corresponding markers are EGF or anti-EGFR antibody, transferrin; floate; RGD, and sulfatide, separately. Recently, brain tumor stem cells (BTSCs) were found to have extraordinary potential to initiate and maintain brain tumors, [83,84]. BTSCs are the driving force of tumor growth, making tumors resistant to radiotherapy and chemotherapy. Therefore, it is important to eliminate BTSCs for the treatment of brain tumors [85]. Identification of the markers of BTSCs will provide a good target to kill tumor cells in the early stage, providing a better therapeutic effect. CD133 is one widely accepted molecular marker expressed in BTSCs but not in bulk tumor cells [83] and can be manipulated as a therapeutic target for nanoparticles to eliminate BTSCs.

4. CONCLUSIONS

Due to non-toxicity and convenient modification, the utilization of nanoparticles as potential targeted vectors for delivering contrast or therapeutic agents to brain tumors has the following advantages [4]: 1. Nanoparticles modified with targeting molecules can pass through the BBB and achieve the delivery of large amounts of therapeutic or imaging agents to tumor cells, although the selective delivery of nanoparticles to tumor is sometimes achieved due to the leaky tumor vasculature, which is known as the EPR effect [86]. 2. A hydrophilic coating and the nanoparticle matrix provide reduced uptake by the RES and provide protection of active agents from environmental degradation, resulting in increased delivery of the nanoparticles to tumor sites and reduced toxicity. 3. The nanoparti-

cles can alleviate the problems posed by the multi-drug resistance (MDR) of cancer cells against many drugs and reduce immunogenicity and side effects.

The future of nanoparticles lies in multifunctional nanoplatforms, which combine both therapeutic components and multimodality imaging. The development of nanoparticle-based DDS could provide efficient, specific *in vivo* drug delivery without systemic toxicity, and the dose delivered as well as the therapeutic efficacy can be accurately measured noninvasively over time. Although conventional nanoparticles such as liposomes and polymers have been approved for clinical use, there is still a long way to go before newer classes of nanoparticles composed of QDs or metallic particles become a clinical reality. Much remains to be done and many factors need to be optimized, among which are biocompatibility, *in vivo* targeting efficacy, pharmacokinetics, and acute/chronic toxicity.

There are also some concerns about the biosafety and possible side effects of using nanopaticles. Nanotoxicology has emerged as a new area for studying the undesirable effects of nanoparticles [87]. First, the toxicity may come from the material itself, such as CdSe/CdTe in QDs. The modification of QDs renders them more biologically inert for future clinical application. Nanoparticle-based drug delivery for solid brain tumors still has a long way to go, but the strong need for more effective chemotherapeutics will continue to motivate studies on nanoparticles. With the capacity to provide effective targeting, high sensitivity, less toxicity and flexibility, nanoparticle-based drug delivery systems will eventually be able to impact disease diagnosis and patient therapy.

ACKNOWLEDGEMENTS

This work was supported by a Grant-in-aid for Scientific Research from the Ministry of Education, Science, Sports and Culture of Japan and by National Natural Science Foundation of China (No. 81071248).

REFERENCES

[1] DeAngelis, L.M. Brain tumors. *N. Engl. J. Med.,* **2001**, *344*, 114-123.

[2] van Rij, C.M.; Wilhelm, A.J.; Sauerwein, W.A.; van Loenen, A.C. Boron neutron capture therapy for glioblastoma multiforme. *Pharm. World Sci.,* **2005**, *27*, 92-95.

[3] Bao, S.; Wu, Q.; McLendon, R.E.; Hao, Y.; Shi, Q.; Hjelmeland, A.B.; Dewhirst, M.W.; Bigner, D.D.; Rich, J.N. Glioma stem cells promote radioresistance by preferential activation of the DNA damage response. *Nature*, **2006**, *444*, 756-760.

[4] Koo, Y.E.; Reddy, G.R.; Bhojani, M.; Schneider, R.; Philbert, M.A.; Rehemtulla, A.; Ross, B.D.; Kopelman, R. Brain cancer diagnosis and therapy with nanoplatforms. *Adv. Drug Deliv. Rev.,* **2006**, *58*, 1556-1577.

[5] Allen, T.M.; Cullis, P.R. Drug delivery systems: entering the mainstream. *Science*, **2004**, *303*, 1818-1822.

[6] Couvreur, P.; Kante, B.; Crislain, L.; Roland, M.; Speiser, P. Toxicity of polyalkylcyanoacrylate nanoparticles II: doxorubicin-loaded nanoparticles. *J. Pharm. Sci.*, **1982**, *71*, 790-792.

[7] Beck, P.; Kreuter, J.; Reszka, R.; Fichtner, I. Influence of polybutylcyanoacrylate nanoparticles and liposomes on the efficacy and toxicity of anticancer drug mitoxantrone in murine tumour models. *J. Microencapsul.*, **1993**, *10*, 101-114.

[8] Lockman, P.R.; Mumper, R.J.; Khan, M.A.; Allen, D.D. Nanoparticle technology for drug delivery across the blood-brain barrier. *Drug Dev. Ind. Pharm.*, **2002**, *28*, 1-13.

[9] Yoon, T.J.; Kim, J.S.; Kim, B.G.; Yu, K.N.; Cho, M.H.; Lee, J.K. Multifunctional nanoparticles possessing a "magnetic motor effect" for drug or gene delivery. *Angew. Chem. Int. Ed. Engl.*, **2005**, *44*, 1068-1071.

[10] Kataoka, K.; Harada, A.; Nagasaki, Y. Block copolymer micelles for drug delivery: design, characterization and biological significance. *Adv. Drug Deliv. Rev.*, **2001**, *47*, 113-131.

[11] Panyam, J.; Labhasetwar, V. Biodegradable nanoparticles for drug and gene delivery to cells and tissue. *Adv. Drug Deliv. Rev.*, **2003**, *55*, 329-347.

[12] Batist, G.; Ramakrishnan, G.; Rao, C.S.; Chandrasekharan, A.; Gutheil, J.; Guthrie, T.; Shah, P.; Khojasteh, A.; Nair, M.K.; Hoelzer, K.; Tkaczuk, K.; Park, Y.C.; Lee, L.W. Reduced cardiotoxicity and preserved antitumor efficacy of liposome-encapsulated doxorubicin and cyclophosphamide compared with conventional doxorubicin and cyclophosphamide in a randomized, multicenter trial of metastatic breast cancer. *J. Clin. Oncol.*, **2001**, *19*, 3439-3441.

[13] Shenoy, D.; Little, S.; Langer, R.; Amiji, M. Poly(ethylene oxide)- modified poly(β-amino ester) nanoparticles as a pH-sensitive system for tumor-targeted delivery of hydrophobic drugs: Part 2. *In vivo* distribution and tumor localization studies. *Pharm. Res.*, **2005**, *22*, 2107-2114.

[14] Maeda, H.; Wu, J.; Sawa, T.; Matsumura, Y.; Hori, K. Tumor vascular permeability and the EPR effect in macromolecular therapeutics: a review. *J. Control Release*, **2000**, *65*, 271-284.

[15] Sengupta, S.; Eavarone, D.; Capila, I.; Zhao, G.; Watson, N.; Kiziltepe, T.; Sasisekharan, R. Temporal targeting of tumour cells and neovasculature with a nanoscale delivery system. *Nature*, **2005**, *436*, 568-572.

[16] Kingsley, J.D.; Dou, H.; Morehead, J.; Rabinow, B.; Gendelman, H.E.; Destache, C.J. Nanotechnology: a focus on nanoparticles as a drug delivery system. *J. Neuroimmune Pharmacol.*, **2006**, *1*, 340-350.

[17] Kreuter, J. Nanoparticulate systems for brain delivery of drugs. *Adv. Drug Deliv. Rev.*, **2001**, *47*, 65-81.

[18] Chen, Y.; Dalwadi, G.; Benson, H.A. Drug delivery across the blood-brain barrier. *Curr. Drug Deliv.*, **2004**, *1*, 361-376.

[19] Schlageter, K.E.; Molnar, P.; Lapin, G.D.; Groothuis, D.R. Microvessel organization and structure in experimental brain tumors: Microvessel populations with distinctive structural and functional properties. *Microvasc. Res.*, **1999**, *58*, 312-328.

[20] Vajkoczy, P.; Menger, M.D. Vascular microenvironment in gliomas. *Cancer Treat. Res.*, **2004**, *117*, 249-262.

[21] Reddy, J.A.; Allagadda, V.M.; Leamon, C.P. Targeting therapeutic and imaging agents to folate receptor positive tumors. *Curr. Pharm. Biotechnol.*, **2005**, *6*, 131-150.

[22] Cascante, M.; Centelles, J.J.; Veech, R.L.; Lee, W.N.; Boros, L.G. Role of thiamin (vitamin B-1) and transketolase in tumor cell proliferation. *Nutr. Cancer*, **2000**, *36*, 150-154.

[23] Park, J.W.; Benz, C.C.; Martin, F.J. Future directions of liposome- and immunoliposome-based cancer therapeutics. *Semin. Oncol.*, **2004**, *31*, 196-205.

[24] Maurer, N.; Fenske, D.B.; Cullis, P.R. Developments in liposomal drug delivery systems. *Expert Opin. Biol. Ther.*, **2001**, *1*, 923-947.

[25] Jiang, W.; Kim, B.Y.; Rutka, J.T.; Chan, W.C. Advances and challenges of nanotechnology-based drug delivery systems. *Expert Opin. Drug Deliv.*, **2007**, *4*, 621-633.

[26] Carlsson, J.; Kullberg, E.B.; Capala, J.; Sjöberg, S.; Edwards, K.; Gedda, L. Ligand liposomes and boron neutron capture therapy. *J. Neurooncol.*, **2003**, *62*, 47-59.

[27] Sofou, S.; Sgouros, G. Antibody-targeted liposomes in cancer therapy and imaging. *Expert Opin. Drug Deliv.*, **2008**, *5*, 189-204.

[28] Maruyama, K. PEG-immunoliposome. *Biosci. Rep.*, **2002**, *22*, 251-266.

[29] Hansen, C.B.; Kao, G.Y.; Moase, E.H.; Zalipsky, S.; Allen, T.M. Attachment of antibodies to sterically stabilized liposomes-evaluation, comparison and optimization of coupling procedures. *Biochim. Biophys. Acta*, **1995**, *1239*, 133-144.

[30] Allen, T.M.; Brandeis, E.; Hansen, C.B.; Kao, G.Y.; Zalipsky, S. A new strategy for attachment of antibodies to sterically stabilized liposomes resulting in efficient targeting to cancer-cells. *Biochim. Biophys. Acta*, **1995**, *1237*, 99-108.

[31] Sapra, P.; Tyagi, P.; Allen, T.M. Ligand-targeted liposomes for cancer treatment. *Curr. Drug Deliv.*, **2005**, *2*, 369-381.

[32] Park, J.W.; Hong, K.; Kirpotin, D.B.; Colbern, G.; Shalaby, R.; Baselga, J.; Shao, Y.; Nielsen, U.B.; Marks, J.D.; Moore, D.; Papahadjopoulos, D.; Benz, C.C. Anti-HER2 immunoliposomes: enhanced efficacy attributable to targeted delivery. *Clin. Cancer Res.*, **2002**, *8*, 1172-1181.

[33] Gabizon, A.; Papahadjopoulos, D. The role of surface charge and hydrophilic groups on liposome clearance *in vivo*. *Biochim. Biophys. Acta*, **1992**, *1103*, 94-100.

[34] Unezaki, S.; Maruyama, K.; Takahashi, N.; Koyama, M.; Yuda, T.; Suginaka, A.; Iwatsuru, M. Enhanced delivery and antitumor activity of doxorubicin using long-circulating thermosensitive liposomes containing amphipathic polyethylene glycol in combination with local hyperthermia. *Pharm. Res.*, **1994**, *11*, 1180-1185.

[35] Friedman, H.S.; Bigner, D.D. Glioblastoma multiforme and the epidermal growth factor receptor. *N. Engl. J. Med.*, **2005**, *353*, 1997-1999.

[36] Schwechheimer, K.; Huang, S.; Cavenee, W.K. EGFR gene amplification-rearrangement in human glioblastomas. *Int. J. Cancer*, **1995**, *62*, 145-148.

[37] Sauter, G.; Maeda, T.; Waldman, F.M.; Davis, R.L.; Feuerstein, B.G. Patterns of epidermal growth factor receptor amplification in malignant gliomas. *Am. J. Pathol.*, **1996**, *148*, 1047-1053.

[38] Ishida, T.; Iden, D.L.; Allen, T.M. A combinatorial approach to producing sterically stabilized (Stealth) immunoliposomal drugs. *FEBS Lett.*, **1999**, *460*, 129-133.

[39] Iden, D.L.; Allen, T.M. *In vitro* and *in vivo* comparison of immunoliposomes made by conventional coupling techniques with those made by a new post-insertion approach. *Biochim. Biophys. Acta*, **2001**, *1513*, 207-216.

[40] Caruso, G.; Raudino, G.; Caffo, M.; Alafaci, C.; Granata, F.; Lucerna, S.; Salpietro, F.M.; Tomasello, F. Nanotechnology Platforms in Diagnosis and Treatment of Primary Brain Tumors. *Recent. Pat. Nanotechnol.*, **2010**, *4*, 119-124.

[41] Hofheinz, R.D.; Gnad-Vogt, S.U.; Beyer, U.; Hochhaus, A. Liposomal encapsulated anti-cancer drugs. *Anticancer Drugs*, **2005**, *16*, 691-707.

[42] Orringer, D.A.; Koo, Y.E.; Chen, T.; Kopelman, R.; Sagher, O.; Philbert, M.A. Small solutions for big problems: the application of nanoparticles to brain tumor diagnosis and therapy. *Clin. Pharmacol. Ther.*, **2009**, *85*, 531-534.

[43] Barth, R.F.; Coderre, J.A.; Vicente, M.G.; Blue, T.E. Boron neutron capture therapy of cancer: current status and future prospects. *Clin. Cancer Res.*, **2005**, *11*, 3987-4002.

[44] Yanagië, H.; Ogata, A.; Sugiyama, H.; Eriguchi, M.; Takamoto, S.; Takahashi, H. Application of drug delivery system to boron neutron capture therapy for cancer. *Expert Opin. Drug Deliv.*, **2008**, *5*, 427-443.

[45] Pan, X.Q.; Wang, H.; Lee, R.J. Boron delivery to a murine lung carcinoma using folate receptor-targeted liposomes. *Anticancer Res.*, **2002**, *22*, 1629-1633.

[46] Doi, A.; Kawabata, S.; Iida, K.; Yokoyama, K.; Kajimoto, Y.; Kuroiwa, T.; Shirakawa, T.; Kirihata, M.; Kasaoka, S.; Maruyama, K.; Kumada, H.; Sakurai, Y.; Masunaga, S.; Ono, K.; Miyatake, S. Tumor specific targeting of sodium borocaptate (BSH) to malignant glioma by transferrin-PEG liposomes: a modality for boron neutron capture therapy. *J. Neurooncol.*, **2008**, *87*, 287-294.

[47] Feng, B.; Tomizawa, K.; Michiue, H.; Miyatake, S.; Han, X.J.; Fujimura, A.; Seno, M.; Kirihata, M.; Matsui, H. Delivery of sodium borocaptate to glioma cells using immunoliposome conjugated with anti-EGFR antibodies by ZZ-*His*. *Biomaterials*, **2009**, *30*, 1746-1755.

[48] Feng, B.; Tomizawa, K.; Michiue, H.; Han, X.J.; Miyatake, S.; Matsui, H. Development of a bifunctional immunoliposome system for combined drug delivery and imaging *in vivo*. *Biomaterials*, **2010**, *31*, 4139-4145.

[49] Martin, B.; Sainlos, M.; Aissaoui, A.; Oudrhiri, N.; Hauchecorne, M.; Vigneron, J.P.; Lehn, J.M.; Lehn, P. The design of cationic lipids for gene delivery. *Curr. Pharm. Des.*, **2005**, *11*, 375-394.

[50] Wasungu, L.; Hoekstra, D. Cationic lipids, lipoplexes and intracellular delivery of genes. J. Control Release, **2006**,116, 255-264.

[51] Gao, X.; Huang, L. Cationic liposome-mediated gene transfer. *Gene Ther.*, **1995**, *2*, 710-722.

[52] Felgner, P.L. Improvements in cationic liposomes for *in vivo* gene transfer. *Hum. Gene Ther.*, **1996**, *7*, 1791-1793.

[53] Voges, J.; Weber, F.; Reszka, R.; Sturm, V.; Jacobs, A.; Heiss, W.D.; Wiestler, O.; Kapp, J.F. Clinical protocol. Liposomal gene therapy with the herpes simplex thymidine kinase gene/ganciclovir system for the treatment of glioblastoma multiforme. *Hum. Gene Ther.*, **2002**, *13*, 675-685.

[54] Yoshida, J.; Mizuno, M.; Clinical gene therapy for brain tumors. Liposomal delivery of anticancer molecule to glioma. *J. Neurooncol.*, **2003**, *65*, 261-267.

[55] Yoshida, J.; Mizuno, M.; Fujii, M.; Kajita, Y.; Nakahara, N.; Hatano, M.; Saito, R.; Nobayashi, M.; Wakabayashi, T. Human gene therapy for malignant gliomas (glioblastoma multiforme and anaplastic astrocytoma) by *in vivo* transduction with human interferon beta gene using cationic liposomes. *Hum. Gene Ther.*, **2004**, *15*, 77-86.

[56] Zhang, Y.; Boado, R.J.; Pardridge, W.M. *In vivo* knockdown of gene expression in brain cancer with intravenous RNAi in adult rats. *J. Gene Med.*, **2003**, *5*, 1039-1045.

[57] Lavasanifar, A.; Samuel, J.; Kwon, G.S. Poly(ethylene oxide)- block -poly(L -amino acid) micelles for drug delivery. *Adv. Drug Deliv. Rev.*, **2002**, *54*, 169-190.

[58] Sahoo, S.K.; Labhasetwar, V. Nanotech approaches to drug delivery and imaging. *Drug Discov. Today*, **2003**, *8*, 1112-1120.

[59] Ong, B.Y.; Ranganath, S.H.; Lee, L.Y.; Lu, F.; Lee, H.S.; Sahinidis, N.V.; Wang, C.H. Paclitaxel delivery from PLGA foams for controlled release in post-surgical chemotherapy against glioblastoma multiforme. *Biomaterials*, **2009**, *30*, 3189-3196.

[60] Xie, J.; Wang, C.H. Electrospun micro- and nanofibers for sustained delivery of paclitaxel to treat C6 glioma *in vitro*. *Pharm. Res.*, **2006**, *23*, 1817-1826.

[61] Haag, R. Supramolecular drug-delivery systems based on polymeric core-shell architectures. *Angew. Chem. Int. Ed. Engl.*, **2004**, *43*, 278-282.

[62] Huang, R.Q.; Ke, W.L.; Qu, Y.H.; Zhu, J.H.; Pei, Y.Y.; Jiang, C. Characterization of lactoferrin receptor in brain endothelial capillary cells and mouse brain. *J. Biomed. Sci.*, **2007**, *14*, 121-128.

[63] Hu, K.; Li, J.; Shen, Y.; Lu, W.; Gao, X.; Zhang, Q.; Jiang, X. Lactoferrin-conjugated PEG-PLA nanoparticles with improved brain delivery: *in vitro* and *in vivo* evaluations. *J. Control Release*, **2009**, *134*, 55-61.

[64] Schottelius, M.; Laufer, B.; Kessler, H.; Wester, H.J. Ligands for mapping alphavbeta3-integrin expression *in vivo*. *Acc. Chem. Res.*, **2009**, *42*, 969-980.

[65] Zhan, C.; Gu, B.; Xie, C.; Li, J.; Liu, Y.; Lu, W. Cyclic RGD conjugated poly(ethylene glycol)-co-poly(lactic acid) micelle enhances paclitaxel anti-glioblastoma effect. *J. Control Release*, **2010**,*143*, 136-142.

[66] Petri, B.; Bootz, A.; Khalansky, A.; Hekmatara, T.; Müller, R.; Uhl, R.; Kreuter, J.; Gelperina, S.; Chemotherapy of brain tumour using doxorubicin bound to surfactant-coated poly(butyl cyanoacrylate) nanoparticles: revisiting the role of surfactants. *J. Control Release*, **2007**, *117*, 51-58.

[67] Zhang, Y.; Sun, C.; Kohler, N.; Zhang, M. Self-assembled coatings on individual monodisperse magnetite nanoparticles for efficient intracellular uptake. *Biomed. Microdevices*, **2004**, *6*, 33-40.

[68] Neuwelt, E.A.; Várallyay, P.; Bagó, A.G.; Muldoon, L.L.; Nesbit, G.; Nixon, R. Imaging of iron oxide nanoparticles by MR and light microscopy in patients with malignant brain tumors, *Neuropathol. Appl. Neurobiol.*, **2004**, *30*, 456-471.

[69] Murillo, T.P.; Sandquist, C.; Jacobs, P.M.; Nesbit, G.; Manninger, S.; Neuwelt, E.A. Imaging brain tumors with ferumoxtran-10, a nanoparticle magnetic resonance contrast agent. *Therapy*, **2005**, *2*, 871-882.

[70] Xu, H.; Song, T.; Bao, X.; Hu, L. Site-directed research of magnetic nanoparticles in magnetic drug targeting. *J. Magn. Magn. Mater.*, **2005**, *293*, 514-519.

[71] Dobson, J. Gene therapy progress and prospects: magnetic nanoparticle-based gene delivery. *Gene Ther.*, **2006**, *13*, 283-287.

[72] Jordan, A.; Scholz, R.; Maier-Hauff, K.; van Landeghem, F.K.; Waldoefner, N.; Teichgraeber, U.; Pinkernelle, J.; Bruhn, H.; Neumann, F.; Thiesen, B.; von Deimling, A.; Felix, R. The effect of thermotherapy using magnetic nanoparticles on rat malignant glioma. *J. Neurooncol.*, **2006**, *78*, 7-14.

[73] Maier-Hauff, K.; Rothe, R.; Scholz, R.; Gneveckow, U.; Wust, P.; Thiesen, B.; Feussner, A.; von Deimling, A.; Waldoefner, N.; Felix, R.; Jordan, A. Intracranial thermotherapy using magnetic nanoparticles combined with external beam radiotherapy: results of a feasibility study on patients with glioblastoma multiforme. *J. Neurooncol.*, **2007**, *81*, 53-60.

[74] Yamada, T.; Iwasaki, Y.; Tada, H.; Iwabuki, H.; Chuah, M.K.; VandenDriessche, T.; Fukuda, H.; Kondo, A.; Ueda, M.; Seno, M.; Tanizawa, K.; Kuroda, S. Nanoparticles for the delivery of genes and drugs to human hepatocytes. *Nat. Biotechnol.*, **2003**, *21*, 885-890.

[75] Yu, D.; Fukuda, T.; Tuoya, Kuroda, S.; Tanizawa, K.; Kondo, A.; Ueda, M.; Yamada, T.; Tada, H.; Seno, M. Engineered bio-nanocapsules, the selective vector for drug delivery system. *IUBMB Life*, **2006**, *58*, 1-6.

[76] Tsutsui, Y.; Tomizawa, K.; Nagita, M.; Michiue, H.; Nishiki, T.; Ohmori, I.; Seno, M.; Matsui, H. Development of bionanocapsules targeting brain tumors. *J. Control Release*, **2007**, *122*, 159-164.

[77] van Vlerken, L.E.; Amiji, M.M. Multi-functional polymeric nanoparticles for tumour-targeted drug delivery. *Expert Opin. Drug Deliv.*, **2006**, *3*, 205-216.

[78] Reddy, G.R.; Bhojani, M.S.; McConville, P.; Moody, J.; Moffat, B.A.; Hall, D.E.; Kim, G.; Koo, Y.E.; Woolliscroft, M.J.; Sugai, J.V.; Johnson, T.D.; Philbert, M.A.; Kopelman, R.; Rehemtulla, A.; Ross, B.D. Vascular targeted nanoparticles for imaging and treatment of brain tumors. *Clin. Cancer Res.*, **2006**, *12*, 6677-6686.

[79] Weng, K.C.; Noble, C.O.; Papahadjopoulos-Sternberg, B.; Chen, F.F.; Drummond, D.C.; Kirpotin, D.B.; Wang, D.; Hom, Y.K.; Hann, B.; Park, J.W. Targeted tumor cell internalization and imaging of multifunctional quantum dot-conjugated immunoliposomes *in vitro* and *in vivo*. *Nano Lett.*, **2008**, *8*, 2851-2857.

[80] Mulder, W.J.; Koole, R.; Brandwijk, R.J.; Storm, G.; Chin, P.T.; Strijkers, G.J.; de Mello Donegá, C.; Nicolay, K.; Griffioen, A.W. Quantum dots with a paramagnetic coating as a bimodal molecular imaging probe. *Nano Lett.*, **2006**, *6*, 1-6.

[81] Derfus, A.M.; Chan, W.C.W.; Bhatia, S.N. Probing the cytotoxicity of semiconductor quantum dots. *Nano Lett.*, **2004**, *4*, 11-18.

[82] Shao, K.; Hou, Q.; Duan, W.; Go, M.L.; Wong, K.P.; Li, Q.T. Intracellular drug delivery by sulfatide-mediated liposomes to gliomas. *J. Control Release*, **2006**, *115*, 150-157.

[83] Singh, S.K.; Hawkins, C.; Clarke, I.D.; Squire, J.A.; Bayani, J.; Hide, T.; Henkelman, R.M.; Cusimano, M.D.; Dirks, P.B. Identification of human brain tumor initiating cells. *Nature*, **2004**, *432*, 396-401.

[84] Vescovi, A.L.; Galli, R.; Reynolds, B.A. Brain tumor stem cells. *Nat. Rev. Cancer*, **2006**, *6*, 425-436.

[85] Mao, X.G.; Zhang, X.; Zhen, H.N. Progress on potential strategies to target brain tumor stem cells. *Cell Mol. Neurobiol.*, **2009**, *29*, 141-155.

[86] Maeda, H. The enhanced permeability and retention (EPR) effect in tumor vasculature: the key role of tumor-selective macromolecular drug targeting, *Adv. Enzyme Regul.*, **2001**, *41*, 189-207.

[87] Kagan, V.E.; Bayir, H.; Shvedova, A.A. Nanomedicine and nanotoxicology: two sides of the same coin. *Nanomedicine*, **2005**, *1*, 313-316.

Received: ?????? 12, 2010 Revised: ?????? 25, 2010 Accepted: ????????? 14, 2010

Biomaterials 31 (2010) 4139–4145

Contents lists available at ScienceDirect

Biomaterials

journal homepage: www.elsevier.com/locate/biomaterials

Development of a bifunctional immunoliposome system for combined drug delivery and imaging *in vivo*

Bin Feng [a,d], Kazuhito Tomizawa [b,*], Hiroyuki Michiue [a], Xiao-Jian Han [a], Shin-ichi Miyatake [c], Hideki Matsui [a]

[a] Department of Physiology, Okayama University Graduate School of Medicine, Dentistry and Pharmaceutical Sciences, 2-5-1 Shikata-cho, Okayama 700-8558, Japan
[b] Department of Molecular Physiology, Faculty of Medical and Pharmaceutical Sciences, Kumamoto University, Kumamoto 860-8558, Japan
[c] Department of Neurosurgery, Osaka Medical College, 2-7 Daigaku-machi, Takatsuki Osaka 569-8686, Japan
[d] Department of Biotechnology, Dalian Medical University, Dalian 116044, China

ARTICLE INFO

Article history:
Received 16 October 2009
Accepted 15 January 2010
Available online 10 February 2010

Keywords:
Glioma cells
EGFR
Immunoliposome
Gaussia luciferase
Bioluminescence
Boron neutron capture therapy

ABSTRACT

The diverse characteristics of immunoliposomes provide advantages for utilization in drug delivery systems. In this study, we fused the antibody affinity motif of protein A (ZZ) with *Gaussia* luciferase (GLase). The fused protein conjugated with an anti-epidermal growth factor receptor (EGFR) monoclonal antibody (GLase-ZZ-His-mAb) was effectively delivered into glioma cells expressing an activated EGFR mutant (EGFRvIII) and the bioluminescence was visualized in the cells. Immunoliposomes were further constructed with DSPE-PEG-MAL for covalent GLase-ZZ-His-mAb conjugation. A fluorescence dye (HPTS) encapsulated in immunoliposomes conjugated with GLase-ZZ-His-mAb was effectively delivered into EGFRvIII-expressing glioma cells. In a murine xenograft model of glioma, moreover, specific targeting of the immunoliposomes was visualized in the tumor. This new bifunctional immunoliposome system has the potential for drug delivery and imaging *in vivo*.

1. Introduction

Liposomes, comprised of naturally-occurring non-cytotoxic phospholipids and cholesterols, have been recognized as a potential drug delivery vehicle for three decades [1]. Their ability to encapsulate water-soluble compounds as well as non-toxic nature surpasses that of all other nanomaterial-based drug delivery platforms [2]. Also, by altering lipid composition, size and surface chemistry, liposomes can be developed into multifunctional constructs to meet the tunable requirements of different DDSs, such as combining diagnostic and therapeutic capabilities, thus providing a universal platform that can simultaneously detect, image and target diseased cells [2].

In recent years, targeted liposomes have emerged as viable candidates for tumor imaging and therapy [3,4]. Tumor-targeting ligands, such as antibodies, or receptor ligands such as folate [5], transferrin [6] and epidermal growth factor (EGF) [7], have been used for targeted ^{10}B delivery in boron neutron capture therapy (BNCT). Targeted liposomes provide an advantage over untargeted liposomes not only because of increased localization to tumor sites but also because of increased interaction with the target cell population once at the tumor sites [8]. Immunoliposomes have also been used to deliver contrast agents and radionuclides for diagnostic imaging and therapy [9–12]. Semiconductor quantum dots (ODs) conjugated to liposomes are used for imaging, and the immunoliposomes are successfully observed *in vitro* and *in vivo* [13].

For real-time imaging in small animals, the bioluminescence produced by the enzymatic reaction of a luciferase with a luciferin has been used to non-invasively monitor biological processes [14]. The methods based on a luciferase–luciferin reaction have been applied to the imaging of tumors in mice with firefly luciferase [15], *Renilla* luciferase [16], and *Vargula* luciferase [17]. As a coelenterazine-dependent luciferase, *Gaussia* luciferase (GLase) was cloned from a marine copepod *Gaussia princes* and has recently been validated as a reporter gene for *in vivo* imaging applications [18,19]. Its small size (19.9 kDa) and independence of ATP make it suitable for detecting bioluminescence when fused with another protein [20–22].

We previously used the antibody affinity motif of protein A (ZZ) as an adaptor to conjugate anti-EGFR antibodies to sodium borocaptate (BSH)-encapsulated nickel-liposomes. The formed immunoliposomes effectively and specifically delivered BSH into EGFR-overexpressing glioma cells *in vitro* and *in vivo* [23]. In the

* Corresponding author. Tel.: +81 96 373 5050; fax: +81 96 373 5052.
E-mail address: tomikt@kumamoto-u.ac.jp (K. Tomizawa).

0142-9612/$ – see front matter © 2010 Elsevier Ltd. All rights reserved.
doi:10.1016/j.biomaterials.2010.01.086

present study, ZZ fused with GLase was used not only as an adaptor to conjugate mAb, but also as an imaging component for detection. Two glioma cell lines, PA U87 not expressing EGFR, and U87 ΔEGFR-overexpressing human EGFR variant III (vIII), were employed to evaluate the efficiency with which the fluorescence dye was delivered and imaging was achieved using the immunoliposomes *in vitro* and *in vivo*.

2. Materials and methods

2.1. Lipids and chemicals

DSPE-PEG-MAL (maleimide), DSPE-PEG_{2000}, DOPC and DOPG were purchased from Nippon Oil and Fats (Tokyo, Japan). Cholesterol, chloroform and diethyl ether were acquired from Wako Pure Chemicals (Japan). 8-Hydroxypyrene-1,3,6-trisulfonic acid trisodium salt (HPTS) and Traut's Reagent (2-Iminothiolane.HCl) were purchased from Sigma–Aldrich and Coelenterazine was purchased from NanoLight Technology.

2.2. Cell lines

U87 ΔEGFR and PA U87 glioma cell lines (kindly donated by Professor Webster K. Cavenee of the University of California at San Diego) were used in all experiments. U87 ΔEGFR cells stably express the constitutively active EGFR, EGFRvIII, whereas PA U87 cells express no EGFR. The cells were maintained in Dulbecco's modified Eagle's medium (DMEM) (Invitrogen) with 10% fetal bovine serum (FBS), penicillin and streptomycin at 37 °C in a humidified atmosphere containing 5% CO_2.

2.3. Expression and purification of recombinant GLase-ZZ-His

The pGLuc plasmid was purchased from LUX biotechnology Ltd (Scotland, UK).The GLase gene was amplified from the plasmid using a sense primer (5′-GAGCTCCATGAAACCAACTGAAAACAATG-3′, underline indicates *Sac*I site) and antisense primer (5′-AAGCTTATCACCACCGGCACCCTT-3′, underline indicates *Hind*III site). The PCR product was ligated into the pCR2.1 TOPO vector (Invitrogen), and digested with *Sac*I and *Hind*III. The digested GLase fragment was then inserted between the *Sac*I-*Hind*III site in the ZZ-His expression plasmid [23]. The recombinant plasmid was transformed into *E. coli* BL21 (DE3). The expression and purification of GLase-ZZ-His were performed as described previously [24].

2.4. Conjugation of GLase-ZZ-His with anti-EGFR antibody or FITC

To conjugate GLase-ZZ-His with the anti-EGFR mouse antibody (101-7300-0, Katayama Chemical Inc., Japan), the two were mixed at a molar ratio of 100:1 (GLase-ZZ-His to antibody) in 200 μL of PBS (pH7.4) and rotated at 4 °C for 2 h to yield GLase-ZZ-His-mAb.

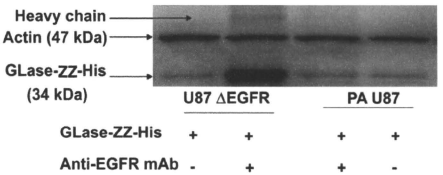

Fig. 1. Antibody-mediated delivery of GLase-ZZ-His into EGFR-overexpressing glioma cells. GLase-ZZ-His-mAb and GLase-ZZ-His were incubated with U87 ΔEGFR and PA U87 for 2 h. After a wash with PBS, cell lysate was subjected to 10% SDS-PAGE and transferred to PVDF membranes. The delivered proteins were detected by Western blotting using anti-His mouse mAb.

For the preparation of FITC-GLase-ZZ-His, GLase-ZZ-His was incubated with 1 mg/mL of fluorescein isothiocyanate isomer I (FITC, Sigma–Aldrich) at room temperature for 15 min with further incubation at 4 °C overnight in PBS as described [25]. The molar ratio of FITC to GLase-ZZ-His was 2:1. After incubation, non-reacted FITC was removed using a PD-10 column (Amersham). To conjugate FITC-GLase-ZZ-His with the anti-EGFR mouse antibody (FITC-GLase-ZZ-His-mAb), the two were mixed at the molar ratio mentioned above.

2.5. Confirmation of the delivery of GLase-ZZ-His-mAb and FITC-GLase-ZZ-His-mAb in cells

PA U87 and U87 ΔEGFR cells were incubated with 3 μM of GLase-ZZ-His-mAb. As a control, the cells were incubated with 3 μM of GLase-ZZ-His. After 2 h, the cells were washed with PBS twice and treated with 0.025% trypsin to remove surface-bound antibody. They were then resuspended in PBS twice before sonication and subjected to Western blotting using an anti-His mouse monoclonal antibody (C-term, Invitrogen). The Western blotting was carried out as described previously [26]. After incubation with the appropriate secondary antibody conjugated with horseradish peroxidase (Sigma–Aldrich), positive bands were visualized using an enhanced chemiluminescence detection system (Amersham Biosciences, Pittsburgh, PA).

After 3 h of incubation with FITC-GLase-ZZ-His-mAb, U87 ΔEGFR and PA U87 cells were washed with PBS twice, then fixed with 4% paraformaldehyde (PFA) for 10 min, and washed with PBS three more times. Fluorescence was observed using

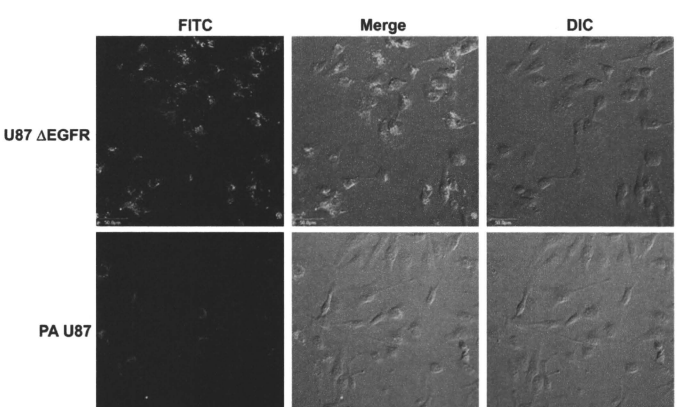

Fig. 2. Fluorescence-based detection of GLase-ZZ-His delivered by the antibody. U87 ΔEGFR and PA U87 cells were incubated with FITC-GLase-ZZ-His-mAb for 2 h and fixed with 4% PFA. Fluorescence was visualized using a confocal laser microscope. Bar = 50 μm.

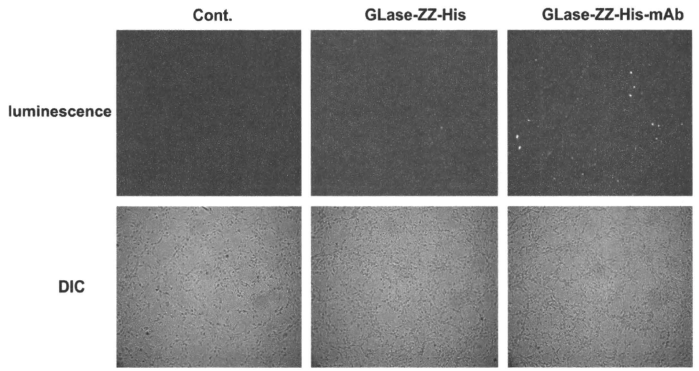

Fig. 3. Bioluminescence-based detection of GLase-ZZ-His in U87 ΔEGFR cells. U87 ΔEGFR cells were incubated with GLase-ZZ-His and GLase-ZZ-His-mAb for 2 h. After being washed with culture medium without serum, the cells were treated with coelenterazine and immediately observed under a bioluminescence microscope.

a confocal laser microscope (FluoView, Olympus, Japan). In the control, only FITC-GLase-ZZ-His was added.

2.6. Bioluminescence imaging of GLase-ZZ-His in cells

To detect the bioluminescence of GLase-ZZ-His, U87 ΔEGFR cells were cultured on a 35-mm glass-bottomed dish for 24–48 h. GLase-ZZ-His-mAb and GLase-ZZ-His were added at 3 μM and the cells were incubated for 2 h, washed with DMEM two times, and soaked with 1 mL of serum-free DMEM containing 1 μg/mL of coelenterazine. Luminescence was immediately recorded with an Olympus Luminoview LV 200 (Bioluminescence microscope (BLM)) after the addition of coelenterazine. Images were acquired and analyzed with Metamorph software (Molecular devices).

2.7. Construction of GLase-ZZ-His-immunoliposomes

Liposomes composed of DOPC: DOPG: CH: DSPE-PEG-MAL: DSPE-PEG_{2000} (3:3:4:0.1:0.1, molar ratio) were prepared by lipid film hydration as described previously with a slight modification [27]. Briefly, 100 μmol of lipid dissolved in 2 mL of a chloroform/diethyl ether mixture (1:1 v/v) was added to a rotary evaporator to form a lipid film under reduced pressure. Two milliliters of PBS containing 35 mM HPTS was then added and the lipid film was vortexed. To control size and lamellarity, the suspension was sonicated by a tip-type ultrasonic homogenizer (output level 7, TAITEC ULTRS Homogenizer VP-5S, Tokyo, Japan) for 5 × 1 min with 1 min ice cooling interval between each round. Then the liposome emulsion was extruded 10 times through a polycarbonate membrane 100 nm in pore size using an extruder device at 50 °C. The mean diameter of the prepared liposomes was determined with an electrophoretic light scattering spectrophotometer (ELS-8000, Photal, Tokyo, Japan). Unencapsulated free HPTS was removed by a PD-10 desalting column (Amersham).

For protein thiolation, GLase-ZZ-His was incubated with Traut's reagent at a molar ratio of 1:2 in PBS (pH7.4) with 0.5 M EDTA. After incubation at room temperature for 1 h, the thiolated GLase-ZZ-His was separated using a PD-10 column, and the fractions containing thiolated GLase-ZZ-His were pooled. Under a nitrogen atmosphere, HPTS-loaded liposomes containing DSPE-PEG_{2000}-maleimide were incubated with thiolated GLase-ZZ-His (molar ratio of DSPE-PEG_{2000}-maleimide to GLase-ZZ-His, 40:1) overnight at room temperature at a low rotating speed [28]. Free GLase-ZZ-His was removed with a Sepharose CL-4B column (1 × 10 cm) and the eluted GLase-ZZ-His-liposomes (Hereafter abbreviate as pre-immunoliposomes) were concentrated and the protein concentration was measured with a Biadford protein assay (Bio-rad). For constructing the immunoliposomes conjugated with anti-EGFR mouse antibody (mAb), the antibody was mixed with pre-immunoliposomes at a molar ratio of 1:20 (mAb to GLase-ZZ-His) at 4 °C with rotation for 2 h. Free mAbs were removed with a Sepharose CL-4B column. The lipid in each fraction was analyzed by the DAOS method using a Phospholipids C reagent kit (Wako Pure Chemical Inc. Ltd., Japan)

2.8. Fluorescence signal and luciferase detection in immunoliposome-treated cells

U87 ΔEGFR cells were cultured on laminin (20 μg/mL)-coated 3 cm dishes (2 mL medium) for 24–48 h, after which immunoliposomes and pre-immunoliposomes were added. The final concentrations of liposome (total lipid), GLase-ZZ-His, and antibody were 1 mM, 2 μM, and 3 μg/mL, respectively. After 2 h incubation, the cells were washed with DMEM twice, fixed with 4% PFA for 10 min, and washed with PBS twice again. Fluorescence signals were observed using a confocal laser microscope. For the detection of GLase-ZZ-His in immunoliposome-treated cells, U87 ΔEGFR cells were washed with DMEM and bioluminescence signals were analyzed as mentioned in 2.6.

2.9. Bioluminescence imaging in vivo

U87 ΔEGFR cells (1×10^6 cells/100 μL) were implanted into the back of female 4-to-6 week-old nude mice (15–20 g, BALB/c Slc-nu/nu; Japan SLC). After 10–14 days, animals bearing palpable tumors were administered intravenously 400 μL of immunoliposomes and pre-immunoliposomes via the tail. After 4 h, mice were imaged by injecting 50 μL of coelenterazine solution (100 μg/mL) at the tumor site under anesthesia using a cooled CCD (IVIS, Xenogen, Alameda, CA) camera as described previously [22]. The intensity of the selected region over the tumor was recorded as maximum photons s^{-1} cm^{-2} $steradian^{-1}$. To obtain control signal intensity, same amount of coelenterazine was injected to the site without tumor.

2.10. Slice analysis for determining HPTS's distribution in tumor

The immunoliposome-injected mice were sacrificed soon after bioluminescence imaging and tissues containing the tumor were excised. Sections 10-μm thick were

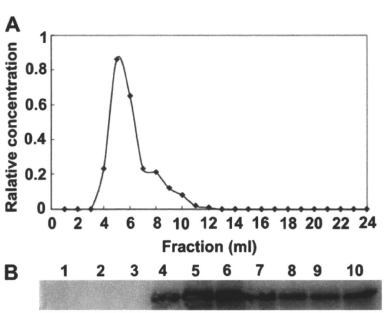

Fig. 4. Characterization of GLase-ZZ-His conjugated to liposomes. (A) GLase-ZZ-His-immunoliposomes (pre-immunoliposomes) were eluted through a Sepharose column and detected by lipid analysis. (B) Ten-microliter aliquots of eluted pre-immunolipo-some samples were subjected to 10% SDS-PAGE and transferred to PVDF membranes. Anti-His mouse monoclonal antibody was used for the detection of GLase-ZZ-His.

cut on a microtome (CM 1850, Leica Microsystems, Wetzlar, Germany) and the fluorescence signal of HPTS was observed immediately using a confocal laser microscope (FluoView, Olympus, Japan).

3. Results

3.1. Delivery of GLase-ZZ-His-mAb into U87 ΔEGFR cells

Little of GLase-ZZ-His was delivered into U87 ΔEGFR cells overexpressing the constitutively active EGFR mutant, EGFRvIII (Fig. 1). When conjugated with the anti-EGFR mouse antibody (GLase-ZZ-His-mAb), however, GLase-ZZ-His was effectively delivered (Fig. 1). In PA U87 cells, which had no EGFR expression, the GLase-ZZ-His level was low even when GLase-ZZ-His was conjugated with the mAb (Fig. 1).

GLase-ZZ-His-mAb was next labelled with FITC and its delivery into U87 ΔEGFR and PA U87 cells was examined using a confocal microscope (Fig. 2). GLase-ZZ-His-mAb was observed in almost all U87 ΔEGFR cells (Fig. 2). A Z-dimensional scan excluded the possibility that the GLase-ZZ-His was attached to the cell surface (Supplementary material). In contrast, weak fluorescence was detected in PA U87 cells (Fig. 2). The results were consistent with those of Western blotting in Fig. 1, and suggest that GLase-ZZ-His was targeted and delivered into the EGFRvIII-overexpressing cells when conjugated with the anti-EGFR antibody.

3.2. Bioluminescence activity of GLase-ZZ-His-mAb in U87 ΔEGFR cells

To clarify whether GLase-ZZ-His had bioluminescence in glioma cells, GLase-ZZ-His was conjugated with the anti-EGFR mAb and added to the culture medium of U87 ΔEGFR cells. A strong signal was detected in the cells (Fig. 3). In GLase-ZZ-His incubated cells, in

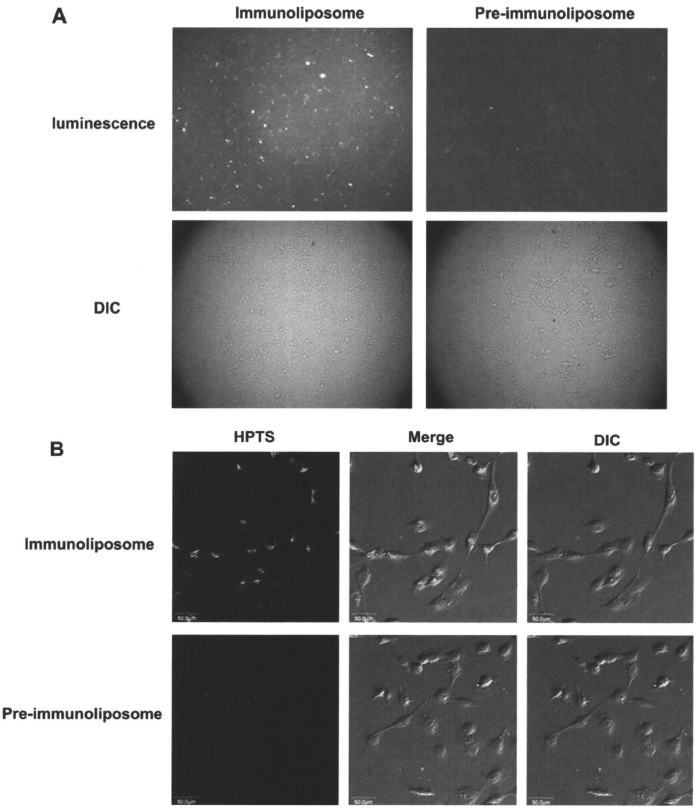

Fig. 5. Bioluminescence and fluorescence-based detection of immunoliposomes delivered into glioma cells. (A) U87 ΔEGFR cells were incubated with immunoliposomes and pre-immunoliposomes for 2 h. After a washing with DMEM, the luminescence was recorded soon after the coelenterazine substrate was added to cells. (B) After the luminescence was observed, the same samples were observed under a confocal microscope to detect fluorescence. Bar = 50 μm.

contrast, weak bioluminescence was detected in a few cells (Fig. 3). The bioluminescence was underdetectable in intact cells (Cont.). These results suggest that the fusion of ZZ-His with GLase did not affect its luciferase function.

3.3. Confirmation of the conjugation of GLase-ZZ-His with pre-immunoliposomes

To investigate whether thiolated GLase-ZZ-His effectively reacted with the maleimide (MAL) group on the liposome's surface, we compared the position of the GLase-ZZ-His and pre-immunoliposome after their separation with Sepharose CL-4B. The peak of the pre-immunoliposome occurred between fractions 5 and 6 (Fig. 4A). Western blotting revealed that GLase-ZZ-His was also abundant in these fractions (Fig. 4B). The results showed that thiolated GLase-ZZ-His was conjugated to the liposome's surface through the MAL-SH group via a covalent reaction. The immunoliposome was eventually produced through conjugation of the anti-EGFR antibody with the pre-immunoliposome.

3.4. Immunoliposome-mediated delivery of HPTS and imaging of GLase-ZZ-His in U87 ΔEGFR cells

To investigate whether immunoliposomes conjugated with the anti-EGFR antibody targeted U87 ΔEGFR cells and are useful for the delivery of chemicals and the imaging of tumors, HPTS, a fluorescence chemical, was encapsulated in the immunoliposome and U87 ΔEGFR cells were incubated with the HPTS-encapsulated immunoliposomes. Strong bioluminescence was detected in the cells (Fig. 5A). In contrast, pre-immunoliposomes not conjugated to the mAb, emitted a faint signal in the cells (Fig. 5A). Moreover, the cells were subjected to fluorescence microscopy. The fluorescence from HPTS was strong in the immunoliposome-treated cells but weak in the pre-immunoliposome-treated cells (Fig. 5B).

3.5. In vivo imaging of xenografted brain tumor using immunoliposomes conjugated with anti-EGFR antibody

We investigated whether the immunoliposomes conjugated with the anti-EGFR antibody could be used to image xenografted brain tumor and carry chemicals. Immunoliposomes and pre-immunoliposomes were injected into the tail of tumor-bearing mice. After 4 h, the tumor was imaged by injection with 50 μL of coelenterazine solution (100 μg/mL) at the tumor site. A strong and clear bioluminescence signal was detected at the tumor site (Fig. 6A, left panel) in immunoliposome-treated mice while weak signals were detected at two tumor sites in the pre-immunoliposome-treated mice (Fig. 6A, right panel). As a signal intensity control, much weaker signal was observed at the site without tumor when coelenterazine was injected (data not shown).

To investigate whether HPTS was specifically carried in the tumor, the tumor xenografted regions were sectioned and the

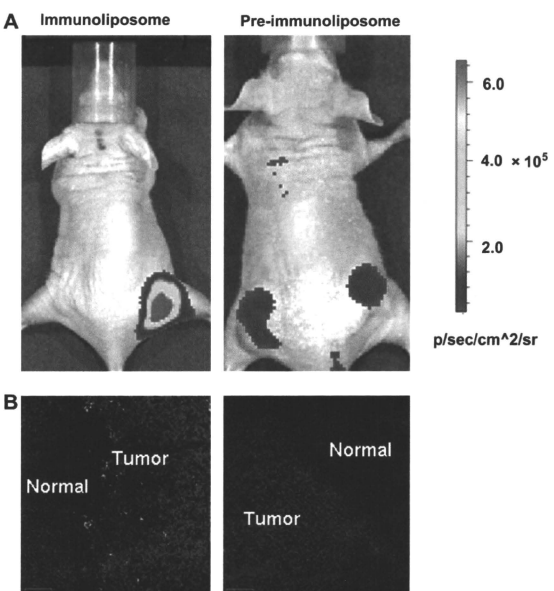

Fig. 6. Bioluminescence imaging in living nude mice harboring U87 ΔEGFR cell xenografts and slice analysis. (A) Images were obtained using a CCD camera 4 h after an intravenous injection of immunoliposomes and pre-immunoliposomes in the tail. A color scale represents p/sec/cm^2/steradian. Left panel, immunoliposome-treated sample. Right panel, pre-immunoliposome-treated sample. (B) A 10-μm section cut from frozen tumor tissue harvested at 4 h post-injection and examined with a confocal microscopy. The tumor section was examined for nuclei stained by Hoechst (blue) and HPTS (green). The blue fluorescence of Hoechst was used to indicate the position of the tumor. Left panel, immunoliposome-treated sample. Right panel, pre-immunoliposome-treated sample. Bar = 200 μm.

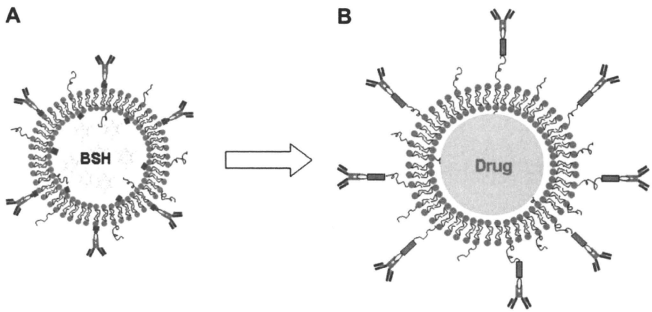

Fig. 7. Development of a bifunctional immunoliposome. (A) Our previous nickel-immunoliposome. (B) The bifunctional immunoliposome.

fluorescence from HPTS was observed using a confocal microscope. The fluorescence was located in the tumor but not in normal tissue in the immunoliposomes-treated mice (Fig. 6B, left panel). In the pre-immunoliposome-treated mice, by contrast, no fluorescence was seen in the tumor or normal regions (Fig. 6B, right panel).

4. Discussion

In the present study, we showed that a fusion protein consisting of ZZ-linked to *Gaussia* luciferase could be used to target and image glioblastoma cells expressing the activated EGFR mutant EGFRvIII. The results support our previous findings obtained with a ZZ conjugated to liposomes for targeting and delivering BSH [23]. Previously, a nickel lipid was used for binding His-tagged ZZ (Fig. 7A) [23]. To avoid possible toxic effects of DOGS-NTA-Ni, we replaced it with DSPE-PEG-MAL for the covalent reaction to conjugate GLase-ZZ-His with the liposome in the present study. Thus, GLase-ZZ-His was located at the distal end of the immunoliposome. The antibody conjugated to ZZ is thought to be located further out than in our previous immunoliposome (Fig. 7B). The design of the new immunoliposome may improve the antibody's ability to recognize and bind tumor cells. Moreover, the usage of an appropriate ratio of DSPE-PEG_{2000} made the immunoliposome more stable. Since the mid-1990s, to increase specific binding while also retaining a long period of circulation, researchers have attached an antibody or ligand to PEG's terminus via a thioether bond [28,29]. This design is used widely by researchers [28,29], but the effect of the thiolation reaction on the stability and affinity of the antibody has not been discussed. In the present study, we followed the same basic design but made some improvements. That is, the antibody was conjugated to PEG via the adaptor GLase-ZZ-His, and remained intact because its Fc part bound with ZZ. The construction of the new immunoliposome prevents shorter circulation times using a complete antibody, due to the rapid identification and uptake of the Fc fragment by macrophages in circulation *in vivo* [30].

In recent years, *Gaussia* luciferase has mostly been used for non-invasive studies because of its high quantum yield compared with firefly luciferase and *Renilla* luciferase [31]. GLase has been used to image cultured cells implanted subcutaneously into nude mice [32]. A recent study showed that GLase fused with an anti-carcinoembryomic antigen (CEA) fragment was capable of targeting and imaging human colon carcinoma cells in nude mice [22]. However, its utilization for detecting the distribution of immunoliposomes has not been reported. In the present study, immunoliposomes conjugated with GLase-ZZ-His and anti-EGFR antibody were used to target and image EGFRvIII-expressing glioma cells both *in vitro* and *in vivo*. Although the luciferase signal was detected at the tumor site by a direct coelenterazine solution injection, the signal intensity is much stronger than those in pre-immunoliposome-treated sample (Fig. 6) and at the site without tumor (data not shown), indicating the GLase on immunoliposome targeted to the tumor site by ZZ conjugated antibody. These results suggest that the bioluminescence of GLase is not affected by thiolation and immunoliposomes conjugated with GLase may be useful for the imaging of tumor cells expressing EGFR. The monitoring of liposomes *in vivo* provides valuable information on drug delivery although the development of this technology is still in its early stages.

The combination of a diagnostic test and a therapeutic entity is termed theranostics [33]. Some chemotherapeutics have been directly or indirectly radiolabeled for single photon emission computed tomography (SPECT) and positron emission tomography (PET) imaging [34]. The radiolabeled chemotherapeutics have been injected into patients for the purpose of better understanding their biodistribution and metabolism and to assess whether there exists a relationship between their uptake in tumor tissue and response to treatment [34]. In the present study, our bifunctional immunoliposomes effectively delivered their cargo to the tumor and also were imaged in nude mice. The present results suggest our bifunctional immunoliposomes to be useful for BNCT as a theranostics reagent.

5. Conclusions

The present study showed the utility of bifunctional immunoliposomes fused with GLase-ZZ-His-mAb for the imaging and targeting of glioma cells both *in vitro* and *in vivo*. A thiolated fusion protein of ZZ (Fc-affinity domain) and GLase was conjugated to the immunoliposomes for antibody binding and imaging. We have demonstrated the utility of *Gaussia princeps* luciferase for detecting the distribution of immunoliposomes. Bioluminescence and fluorescence analyses indicated that GLase-ZZ-His and HPTS were successfully delivered into EGFR-overexpressing glioma cells *in vitro* and *in vivo*. Thus, our bifunctional immunoliposome system provides the potential for drug delivery and imaging in tumors.

Acknowledgements

This work was supported by a Grant-in-aid for Scientific Research from the Ministry of Education, Science, Sports and

Culture of Japan and by a Grant-in-aid for Scientific Research from the Ministry of Health, Labour and Welfare of Japan.

Supplementary data

Supplementary material associated with this paper can be found, in the online version, at doi:10.1016/j.biomaterials.2010.01.086

Appendix

Figures with essential colour discrimination. Certain figures in this article, in particular Figs. 4 and 7, that are difficult to interpret in black and white. The full colour images can be found in the online version, at doi:10.1016/j.biomaterials.2010.01.086

References

[1] Maurer N, Fenske DB, Cullis PR. Developments in liposomal drug delivery systems. Expert Opin Biol Ther 2001;1:923–47.
[2] Jiang W, Kim BY, Rutka JT, Chan WC. Advances and challenges of nanotechnology-based drug delivery systems. Expert Opin Drug Deliv 2007;4:621–33.
[3] Elbayoumi TA, Pabba S, Roby A, Torchilin VP. Antinucleosome antibody-modified liposomes and lipid-core micelles for tumor-targeted delivery of therapeutic and diagnostic agents. J Liposome Res 2007;17:1–14.
[4] Sajja HK, East MP, Mao H, Wang YA, Nie S, Yang L. Development of multifunctional nanoparticles for targeted drug delivery and noninvasive imaging of therapeutic effect. Curr Drug Discov Technol 2009;6:43–51.
[5] Pan XQ, Wang H, Lee RJ. Boron delivery to a murine lung carcinoma using folate receptor-targeted liposomes. Anticancer Res 2002;22:1629–33.
[6] Maruyama K, Ishida O, Kasaoka S, Takizawa T, Utoguchi N, Shinohara A, et al. Intracellular targeting of sodium mercaptoundecahydrododecaborate (BSH) to solid tumors by transferrin-PEG liposomes, for boron neutron-capture therapy (BNCT). J Control Release 2004;98:195–207.
[7] Bohl Kullberg E, Bergstrand N, Carlsson J, Edwards K, Johnsson M, Sjöberg S, et al. Development of EGF-conjugated liposomes for targeted delivery of boronated DNA binding agents. Bioconjug Chem 2002;13:737–43.
[8] Sofou S, Sgouros G. Antibody-targeted liposomes in cancer therapy and imaging. Expert Opin Drug Deliv 2008;5:189–204.
[9] Erdogan S, Roby A, Sawant R, Hurley J, Torchilin VP. Gadolinium-loaded polychelating polymer-containing cancer cell-specific immunoliposomes. J Liposome Res 2006;16:45–55.
[10] Kostarelos K, Emfietzoglou D. Tissue dosimetry of liposome-radionuclide complexes for internal radiotherapy: toward liposome-targeted therapeutic radiopharmaceuticals. Anticancer Res 2000;20:3339–45.
[11] Erdogan S, Medarova ZO, Roby A, Moore A, Torchilin VP. Enhanced tumor MR imaging with gadolinium-loaded polychelating polymer-containing tumor-targeted liposomes. J Magn Reson Imaging 2008;27:574–80.
[12] Torchilin VP. Polymeric contrast agents for medical imaging. Curr Pharm Biotechnol 2000;1:183–215.
[13] Weng KC, Noble CO, Papahadjopoulos-Sternberg B, Chen FF, Drummond DC, Kirpotin DB, et al. Targeted tumor cell internalization and imaging of multifunctional quantum dot-conjugated immunoliposomes *in vitro* and *in vivo*. Nano Lett 2008;8:2851–7.
[14] Welsh DK, Kay SA. Bioluminescence imaging in living organisms. Curr Opin Biotechnol 2005;16:73–8.
[15] Swijnenburg RJ, Schrepfer S, Cao F, Pearl JI, Xie X, Connolly AJ, et al. *In vivo* imaging of embryonic stem cells reveals patterns of survival and immune rejection following transplantation. Stem Cells Dev 2008;17:1023–9.
[16] Bhaumik S, Lewis XZ, Gambhir SS. Optical imaging of Renilla luciferase, synthetic Renilla luciferase, and firefly luciferase reporter gene expression in living mice. J Biomed Opt 2004;9:578–86.
[17] Thompson EM, Adenot P, Tsuji FI, Renard JP. Real time imaging of transcriptional activity in live mouse preimplantation embryos using a secreted luciferase. Proc Natl Acad Sci U S A 1995;92:1317–21.
[18] Verhaegent M, Christopoulos TK. Recombinant *Gaussia* luciferase. Overexpression, purification, and analytical application of a bioluminescent reporter for DNA hybridization. Anal Chem 2002;74:4378–85.
[19] Tannous BA. *Gaussia* luciferase reporter assay for monitoring biological processes in culture and *in vivo*. Nat Protoc 2009;4:582–91.
[20] Suzuki T, Usuda S, Ichinose H, Inouye S. Real bioluminescence imaging of a protein secretory pathway in living mammalian cells using *Gaussia* luciferase. FEBS Lett 2007;581:4551–6.
[21] Venisnik KM, Olafsen T, Loening AM, Iyer M, Gambhir SS, Wu AM. Bifunctional antibody-Renilla luciferase fusion protein for *in vivo* optical detection of tumors. Protein Eng Des Sel 2006;19:453–60.
[22] Venisnik KM, Olafsen T, Gambhir SS, Wu AM. Fusion of *Gaussia* luciferase to an engineered anti-carcinoembryonic antigen (CEA) antibody for *in vivo* optical imaging. Mol Imaging Biol 2007;9:267–77.
[23] Feng B, Tomizawa K, Michiue H, Miyatake S, Han XJ, Fujimura A, et al. Delivery of sodium borocaptate to glioma cells using immunoliposome conjugated with anti-EGFR antibodies by ZZ-His. Biomaterials 2009;30:1746–55.
[24] Feng B, Zhao CH, Tanaka S, Imanaka H, Imamura K, Nakanishi K. TPR domain of Ser/Thr phosphatase of *Aspergillus oryzae* shows no auto-inhibitory effect on the dephosphorylation activity. Int J Biol Macromol 2007;41:281–5.
[25] Hashizume T, Fukuda T, Nagaoka T, Tada H, Yamada H, Watanabe K, et al. Cell type dependent endocytic internalization of ErbB2 with an artificial peptide ligand that binds to ErbB2. Cell Biol Int 2008;32:814–26.
[26] Tomizawa K, Iga N, Lu YF, Moriwaki A, Matsushita M, Li ST, et al. Oxytocin improves long-lasting spatial memory during motherhood through MAP kinase cascade. Nat Neurosci 2003;6:384–90.
[27] Kheirolomoom A, Ferrara KW. Cholesterol transport from liposomal delivery vehicles. Biomaterials 2007;28:4311–20.
[28] Béduneau A, Saulnier P, Hindré F, Clavreul A, Leroux JC, Benoit JP. Design of targeted lipid nanocapsules by conjugation of whole antibodies and antibody Fab' fragments. Biomaterials 2007;28:4978–90.
[29] Kirpotin D, Park JW, Hong K, Zalipsky S, Li WL, Carter P, et al. Sterically stabilized anti-HER2 immunoliposomes: design and targeting to human breast cancer cells in vitro. Biochemistry 1997;36:66–75.
[30] Kamps JA, Scherphof GL. Receptor versus non-receptor mediated clearance of liposome. Adv Drug Deliv Rev 1998;32:81–97.
[31] Tannous BA, Kim DE, Fernandez JL, Weissleder R, Breakefield XO. Codon-optimized *Gaussia* luciferase cDNA for mammalian gene expression in culture and *in vivo*. Mol Ther 2005;11:435–43.
[32] Wurdinger T, Badr C, Pike L, de Kleine R, Weissleder R, Breakefield XO, et al. A secreted luciferase for *ex vivo* monitoring of *in vivo* processes. Nat Methods 2008;5:171–3.
[33] Del Vecchio S, Zannetti A, Fonti R, Pace L, Salvatore M. Nuclear imaging in cancer theranostics. Q J Nucl Med Mol Imaging 2007;51:152–63.
[34] Rottey S, Signore A, Van de Wiele C. Radiolabelled chemotherapeutics. Q J Nucl Med Mol Imaging 2007;51:139–51.

Cell-penetrating D-Isomer Peptides of p53 C-terminus: Long-term Inhibitory Effect on the Growth of Bladder Cancer

Daiji Araki, Kentaro Takayama, Miyabi Inoue, Toyohiko Watanabe, Hiromi Kumon, Shiroh Futaki, Hideki Matsui, and Kazuhito Tomizawa

OBJECTIVES To investigate whether a single application of the membrane-permeable D-isomer of the p53 C-terminus connected with a retro-inverso version of the NH_2-terminal 20-amino acid peptide of the influenza virus hemagglutinin-2 protein (riHA2) inhibited the growth of bladder cancer cells. The transduction of p53 using poly-arginine is useful for targeting and suppressing the growth of bladder cancer cells. However, the protein's intracellular half-life is short, and repeated application is necessary to achieve an anti-tumor effect.

METHODS The p53 carboxyl-terminal peptides covalently coupled with cell-penetrating peptides were synthesized with D- or L-amino acids. Moreover, the peptides were connected with riHA2 by a disulfide bridge. Human bladder cancer cell lines were incubated with each peptide and cell viability was assessed with the WST assay. Apoptotic cells were confirmed by Hoechst and active capase-3 staining. The p53 peptides were injected into severe combined immunodeficiency disease mice transplanted with J82 cells to investigate their anti-tumor effect on bladder tumors. A survival curve was plotted using the Kaplan–Meier method.

RESULTS A single application of cell-penetrating D-isomer peptides of the p53 C-terminus connected with riHA2 (d11R-p53C′-riHA2 and dFHV-p53C′-riHA2) inhibited the growth and induced the apoptosis of bladder cancer cells. The tumor-bearing mice treated only with vehicle had a mean survival time of 12 days, whereas treatment with d11R-p53C′-riHA2 resulted in a long-term survival rate of 50%.

CONCLUSIONS Peptide transduction therapy using the D-isomer p53 C-terminal peptide with riHA2 may be an innovative method for the treatment of bladder cancer. UROLOGY 75: 813–819, 2010. © 2010 Elsevier Inc.

There are 2 types of bladder cancer, superficial and invasive. The invasive type is aggressive, with 40%-50% of its cells having mutations in the *p53* tumor suppressor gene. This form of bladder cancer has a poor prognosis despite surgery, chemotherapy, and radiation.[1] New strategies to treat invasive bladder cancer include interleukin-2 gene therapy and adenoviral vector-mediated gene transfer therapy.[2,3] Although gene therapy is a valid option, problems associated with immunogenicity and an insufficient systemic biodistribution to disseminated metastases are likely to curtail its efficacy.[4]

Intracellular protein delivery using membrane-permeable peptide vectors has received increasing attention as a novel and highly efficient way to modify cellular functions with therapeutic potential.[5–7] The vectors are often referred to as cell-penetrating peptides (CPPs) or protein transduction domain (PTD) peptides. Through conjugation with a short peptide vector (<12 amino acid residues) such as the PTD of the human immunodeficiency virus type 1 TAT protein, poly-arginine (6-12 residues), and the PTD derived from flock house virus (FHV), various proteins have been introduced into cells and have successfully exerted their functions.[7,8] Previous studies have demonstrated that the internalization of CPPs and PTD peptides does not involve endocytosis or specific protein transporters,[8–10] and that TAT-PTD fusion proteins are internalized rapidly by lipid raft-dependent macropinocytosis.[11] Eleven poly-arginine (11R)-fused p53 protein (11R-p53) effectively penetrates the plasma membrane of cancer cells.[12,13] The protein inhibits the proliferation of human bladder and oral cancer cells as effectively as adenovirus-mediated p53 gene therapy, but with less cytotoxicity.[12,13] However, a high concentration (>1 μM) and repeated administration of 11R-p53

From the Departments of Physiology and Urology, Okayama University Graduate School of Medicine, Dentistry and Pharmaceutical Sciences, Okayama, Japan; Department of Molecular Physiology, Faculty of Medical and Pharmaceutical Sciences, Kumamoto University, Kumamoto, Japan; and Institute for Chemical Research, Kyoto University, Kyoto, Japan

Reprint requests: Kazuhito Tomizawa, Ph.D., Department of Molecular Physiology, Faculty of Medical and Pharmaceutical Sciences, Kumamoto University, Kumamoto 860-8556, Japan. E-mail: tomikt@kumamoto-u.ac.jp

Submitted: July 6, 2009, accepted (with revisions): October 4, 2009

0090-4295/10/$34.00
doi:10.1016/j.urology.2009.10.002

are needed for transcriptional activation and the growth inhibition of cancer cells.[12] The transduced protein's entrapment in macropinosomes may weaken its effect. The NH_2-terminal 20-amino acid peptide of the influenza virus hemagglutinin-2 protein (HA-2) is well characterized as a pH-sensitive fusogenic peptide that destabilizes lipid membranes at low pH and enhances the release of fusion proteins from macropinosomes.[14,15] Linking HA-2 with 11R-p53 induced the release from macropinosomes of glioma cells and enhanced the anticancer effect of 11R-p53.[16] Such a macropinosome-releasing mechanism would be useful for p53 transduction therapy. However, p53 transduction is still imperfect because the wild-type p53 protein is rapidly degraded by the ubiquitin-proteasome pathway.[17]

The C-terminus of p53 is a lysine-rich domain subject to a variety of posttranslational modifications.[18,19] A peptide derived from the C-terminus activates specific DNA-binding by p53 in vitro through an unknown mechanism.[20] A previous study showed that a transducible D-isomer of this peptide fused with TAT-PTD (TAT-p53C′) activated the p53 protein in cancer cells, significantly increasing lifespan in animal models of terminal peritoneal carcinomatosis and peritoneal lymphoma expressing wild-type *p53*.[21] These results suggest that a proteolysis-resistant and transducible p53 C-terminal peptide would inhibit the growth of bladder cancer. However, the peptide fused with TAT-PTD was not effective enough against cancer cells expressing mutant *p53*.[21] Here we developed a fusion peptide composed of a transducible D-isomer of the C-terminal of p53 (p53C′) and the retro-inverso version of HA-2 (riHA2) peptides, and examined whether it inhibited the growth of bladder cancer cells expressing mutant *p53* and lengthened the survival of mice harboring peritoneal metastasis of bladder cancer.

MATERIAL AND METHODS

Cell Lines and Cultures

The human bladder cancer cell lines J82 and T24 were obtained from American Type Culture Collection. J82 was maintained in MEM (Invitrogen, Carlsbad, CA) supplemented with 10% fetal bovine serum, penicillin (100 U/mL), and streptomycin (100 U/mL). T24 was maintained in McCoy's 5 A medium (Invitrogen) supplemented with 10% fetal bovine serum, penicillin (100 U/mL), and streptomycin (100 U/mL).

Peptide Synthesis

The TAT-p53C′ (RRRQRRKKRGY-GKKHRSTSQGKKSKLHSSHA*RSG*-amide), FHV-p53C (RRRRNRTRRNRRRVRGKKHRSTSQGKKSKLHSSHARSG-amide), 11R-p53C′ (RRRRRRRRRRR-*GKKHRSTSQGKKSKLHSSHARSG*-amide), dFHV-p53C′ (*RRRRNRTRRNRRRVR-GKKHRSTSQGKKSKLHSSHARSG*-amide), and d11R-p53C′ (*RRRRRRRRRRR-GKKHRSTSQGKKSKLHSSHARSG*-amide) peptides (D-amino acids represented in italics) were prepared by standard Fmoc chemistry on a Rink amide resin with purification by HPLC as described previously.[22] For preparation of the dFHV-p53C′-riHA2 peptide, 2 segments, *RRRRNRTRRNRRRVR-GKKHRSTSQGKKSKLHSSHARSG*C-amide and *GDIMGEWGNEIFGAIAGFLG*C-amide (riHA2), prepared by Fmoc chemistry were connected by a disulfide bridge as reported.[23] The dR11-p53C′-riHA2 peptide was similarly prepared by disulfide cross-linking of the corresponding segments, *RRRRRRRRRRR-GKKHRSTSQGKKSKLHSSHARSG*C-amide and *GDIMGEWGNEIFGAIAGFLG*C-amide. The structure of each synthesized peptides was confirmed by mass spectrometry.

Treatment of Bladder Cancer Cells With Each Peptide

In a 96-well dish, 5×10^3 J82 cells and 1×10^3 T24 cells were plated per well. After 24 hours, the cells were incubated with each peptide for 4 hours. They were then washed with phosphate buffer solution (PBS) 3 times, and fresh medium without the peptides was added. The cells were harvested on day 1, 2, 3, and 4 (representing 24 48 72, and 96 hours, respectively, after the start of incubation with each peptide), and the WST-1 assay was performed to assess cell growth.

Cell Viability Assay

Cell viability was determined using a WST-1 (2-[2-methoxy-4-nitrophenyl]-3-[4-nitrophenyl]-5-[2,4-disulfophenyl]-2H-tetrazolium, monosodium salt) assay (Roche Applied Science, Mannheim, Germany) as described previously.[24]

Detection of Apoptotic Cells

Apoptotic cells were identified with Hoechst as described previously.[24] Briefly, J82 and T24 cells seeded in 35-mm diameter culture dishes were incubated with 5 μM CPP-p53C′, dCPP-p53C′ and dCPP-p53C′-riHA2 for 2 hours. After 2 washes with PBS, the cells were further incubated in fresh medium for 24 hours. They were then fixed with 4% parafolmaldehyde. After fixation, the cells were incubated with 0.1 mg/mL of Hoechst 33 248 (Sigma-Aldrich Xhemical, St. Louis, MO) for 1 minute. The morphology of the nucleus was observed with a fluorescence microscope. Apoptotic cells were identified by the presence of highly condensed or fragmented nuclei. Representative graphs are shown for experiments in which at least 6 randomly chosen fields with 100 cells were scored. For active caspase-3 staining, J82 and T24 cells were treated with 5 μM 11R-p53C′, 11R-p53C′, and 11R-p53C′-riHA2 for 2 hours. After being washed with PBS, the cells were further incubated in fresh medium for 24 hours. Immunocytochemistry was then performed using anti-active caspase-3 antibodies (1:200 dilution, R&D Systems, Minneapolis, MN) as described previously.[24] Active caspase-3-positive cells were counted under a confocal laser microscope (FluoView 300, Olympus, Tokyo, Japan). Representative graphs are shown for experiments in which at least 6 randomly chosen fields with 100 cells were scored.

Animal Experiments

The experiments with animals were approved by the Animal Research and Care Committee of Okayama University Graduate School of Medicine, Dentistry and Pharmaceutical Sciences. Female B6 severe combined immunodeficiency disease ($H\text{-}2^b$) mice (8 weeks old) were purchased from CREA Japan (Tokyo, Japan). The mice were anesthetized with pentobarbital sodium (40 mg/kg i.p.) and intraperitoneally injected with J82 cells (2×10^6) in 250 μL of PBS. After 3 days, the mice were intraperitoneally injected with d11R-p53C′-riHA2 (20 mg/kg)

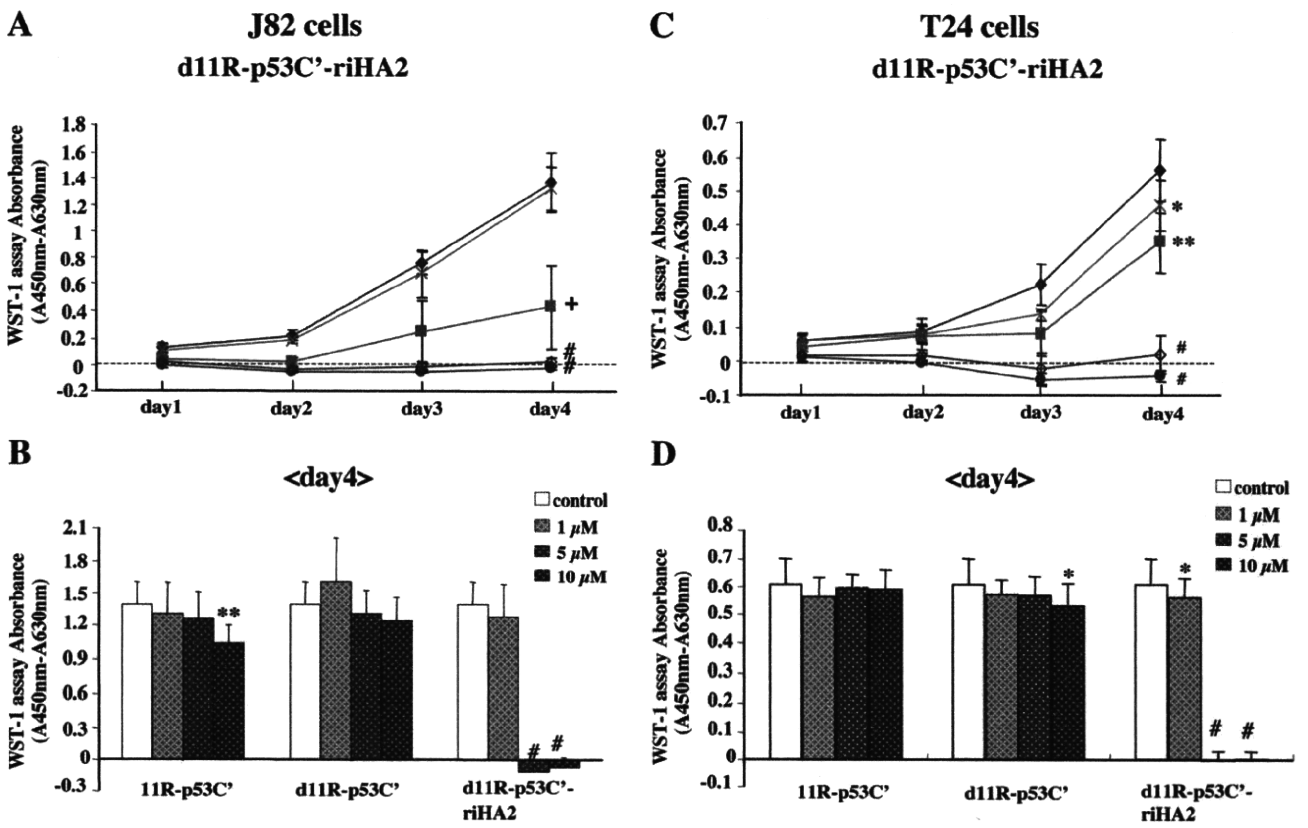

Figure 1. Dose-dependent effect of 11R-p53C′ peptides on the growth of J82 and T24 cells. Time-dependent changes in the growth of J82 (A) and T24 (C) cells treated with different concentrations of d11R-p53C′-riHA2. ◆, Control; ×, 1 μM; ■, 2 μM; ◇, 5 μM; ●, 10 μM. Comparison of the inhibitory effect of each peptide on the growth of J82 (B) and T24 (D) cells. Each concentration of the peptides was applied on day 0. After 96 hours, the cells were harvested and the WST-1 assay was performed. n = 8 each. $^{*}P < .05$, $^{**}P < .01$, $^{+}P < .0005$, and $^{\#}P < 0.0001$ vs control.

in 200 μL of PBS. As a control, the mice were injected with PBS. A survival curve was plotted using the Kaplan–Meijer method (n = 7 for each group).

Statistical Analysis

Data are shown as the mean (± SEM) and were analyzed using either Student t test to compare 2 conditions or analysis of variance followed by planned comparisons of multiple conditions in all experiments except the animal survival experiments. Survival curves were generated according to the Kaplan–Meier method, and differences in survival were analyzed by the Wilcoxon rank-sum test. $P < .05$ was considered significant.

RESULTS

Inhibitory Effect of CPPs-p53C′-riHA2 on the Growth of Bladder Cancer Cells

A previous study showed that a transducible D-isomer of the p53 C-terminus fused with TAT-PTD (TAT-p53C′) significantly inhibited the growth of tumor cells expressing wild-type p53 but not of the cells expressing mutant p53.[21] In the present study, the effect of TAT-p53C′ on the growth of bladder cancer cells expressing mutant p53 was examined. The T24 cell line contains an allele encoding p53 with an in-frame deletion of tyrosine 126, whereas the J82 cell line expresses a *p53* gene mutated in codons 271, 274, and 320.[13] No concentration (1-10 μM) of TAT-p53C′ had an inhibitory effect on the growth of T24 and J82 cells (data not shown).

We next examined whether the other CPPs (11 R and FHV) connected to p53C′ peptides had inhibitory effects on the growth of J82 and T24 cells. To investigate the dose-dependency of the inhibitory effect of p53C′ on the growth of bladder cancer cells, J82 and T24 cells were treated with CPPs-p53C′ (L-amino acid CPPs), dCPPs-p53C′ (D-amino acid CPPs), and dCPPs-p53C′-riHA2. Although 10 μM 11R-p53C′ partially inhibited the growth of J82 cells, lower concentrations of 11R-p53C′ and each concentration of d11R-p53C′ had little effect on the growth of the cells (Fig. 1B). In contrast, HA2-fused D-isomer 11R-p53C′ peptides (d11R-p53C′-riHA2) inhibited the growth of the cells in a dose-dependent manner (Figs. 1A and B). Moreover, 5 and 10 μM d11R-p53C′-riHA2 completely inhibited the growth of J82 cells (Figs. 1A and B). Each peptide had a similar inhibitory effect on the growth of T24 cells (Figs. 1C and D). No concentration of L-isomer 11R-p53C′ (11R-p53C′) had an effect on the growth of T24 cells (Fig. 1D). Low concentrations (1 and 5 μM) of D-isomer 11R-p53C′ (d11R-p53C′) did not affect the growth of T24 cells, whereas 10 μM d11R-p53C′ slightly inhibited cell

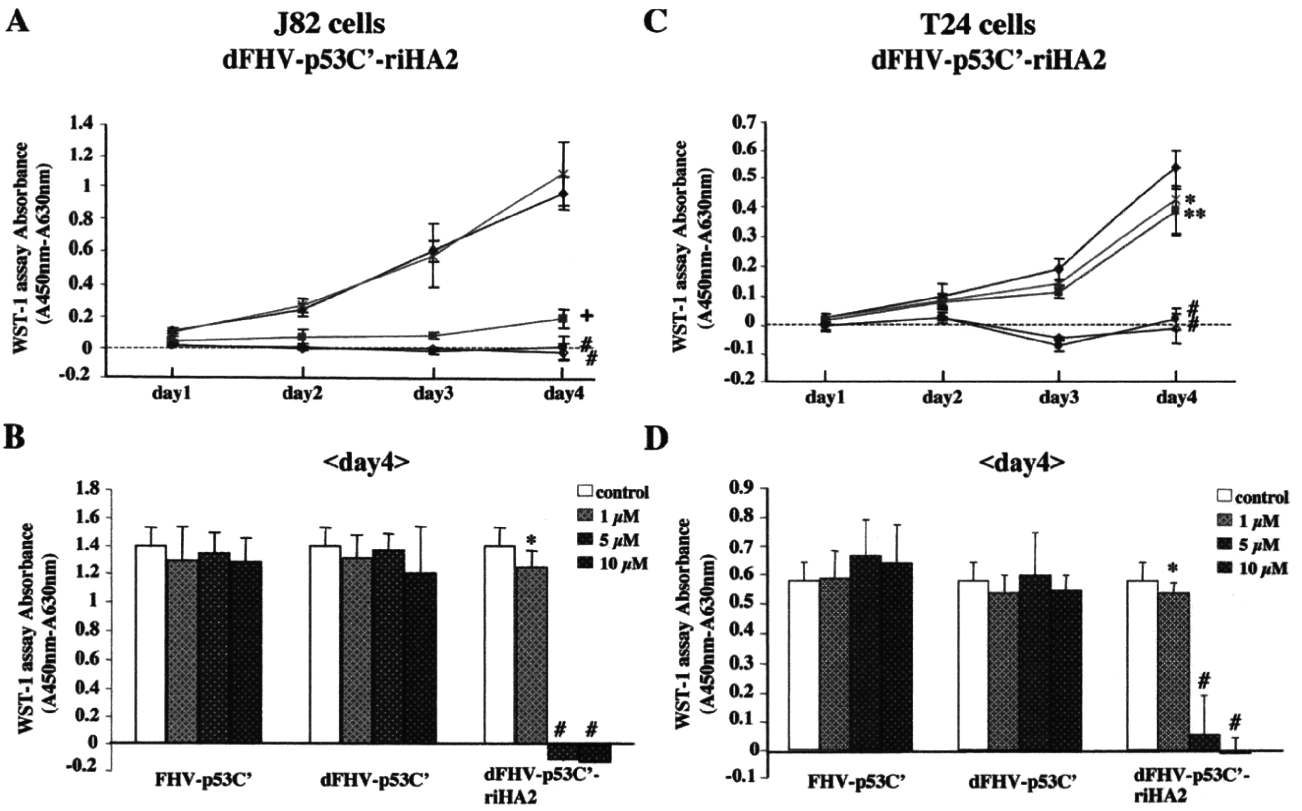

Figure 2. Dose-dependent effect of flock house virus (FHV)-fused p53C′ peptides on the growth of J82 and T24 cells. Time-dependent changes in the growth of J82 (A) and T24 (C) cells treated with different concentrations of dFHV-p53C′-riHA2. ◆, Control; ×, 1 μM; ■, 2 μM; ◇, 5 μM; ●, 10 μM. Comparison of the inhibitory effect of each peptide on the growth of J82 (B) and T24 (D) cells. n = 8 each. $^{*}P < .05$, $^{**}P < .01$, $^{+}P < .0005$ and $^{\#}P < .0001$ vs control.

growth (Fig. 1D). A single application of 5 or 10 μM of d11R-p53C′-riHA2 completely blocked the cell growth (Figs. 1C and D).

Next, the effect of each FHV-fused peptide (FHV-p53′ and dFHV-p53C′) on the growth of J82 and T24 cells was examined (Fig. 2). Neither FHV-p53′ nor dFHV-p53C′ had an inhibitory effect on the growth of T24 and J82 cells (Figs. 2B and D). In contrast, HA2-fused dFHV-p53C′ (dFHV-p53C′-riHA2) dose-dependently inhibited the growth of both cells (Figs. 2A and C). Complete inhibition of the growth of J82 cells and T24 cells was achieved with more than 10 and 5 μM of dR11-p53C′-riHA2, respectively (Figs. 2B and D). To confirm that the inhibition by dCPP-p53C′-riHA2 was not caused by a toxic effect of HA-2, HA-2 peptides fused with R11 (R11-riHA2) were introduced into J82 and T24 cells, and the effect on cell growth was examined. CPPs-riHA2 (5 μM) had no effect on the growth of the bladder cell lines (data not shown).

Induction of Apoptosis of Bladder Cancer Cells by dCPPs-p53C′-riHA2

The ability of each peptide to induce the apoptosis of T24 and J82 cells was examined. The effect of 11R-p53C′ and d11R-p53C′ at 5 μM was weak, with less than 25% of J82 and T24 cells apoptotic (Figs. 3A and B). In contrast, d11R-p53C′-riHA2 at 5 μM significantly induced apoptosis in both cell lines (Figs. 3A and B). Treatment with FHV-fused peptides had the same results. FHV-p53C′ and dFHV-p53C′, with no riHA2, had a weak effect, whereas dFHV-p53-riHA2 markedly induced apoptosis (Figs. 3C and D). Moreover, d11R-p53C′-riHA2 significantly induced the activation of caspase-3 compared with 11R-p53C′ and d11R-p53C′ (Figs. 3E and F).

d11R-p53C′-riHA2 Treatment Leads to Long-term Survival in Mice With Peritoneal Metastasis of Bladder Cancer

Finally, the effect of d11R-p53C′-riHA2 and d11R-p53C′ on survival in an animal model of the peritoneal metastasis of bladder cancer was examined. severe combined immunodeficiency disease mice were intraperitoneally implanted with J82 cells and then injected with 20 mg/kg of d11R-p53C′-riHA2 and d11R-p53C′. The tumor-bearing mice treated only with vehicle had a mean survival time of 12 days, as did the mice treated with d11R-p53C′ ($P = .89$) (Fig. 4). In contrast, treatment with d11R-p53C′-riHA2 resulted in a long-term survival rate of 50% ($P = .005$ 22 vs vehicle, and $P = .007$ 42 vs d11R-p53C′), and no mice injected with the peptide showed overt symptoms of tumor morbidity 18 days after the tumor cells were implanted (Fig. 4).

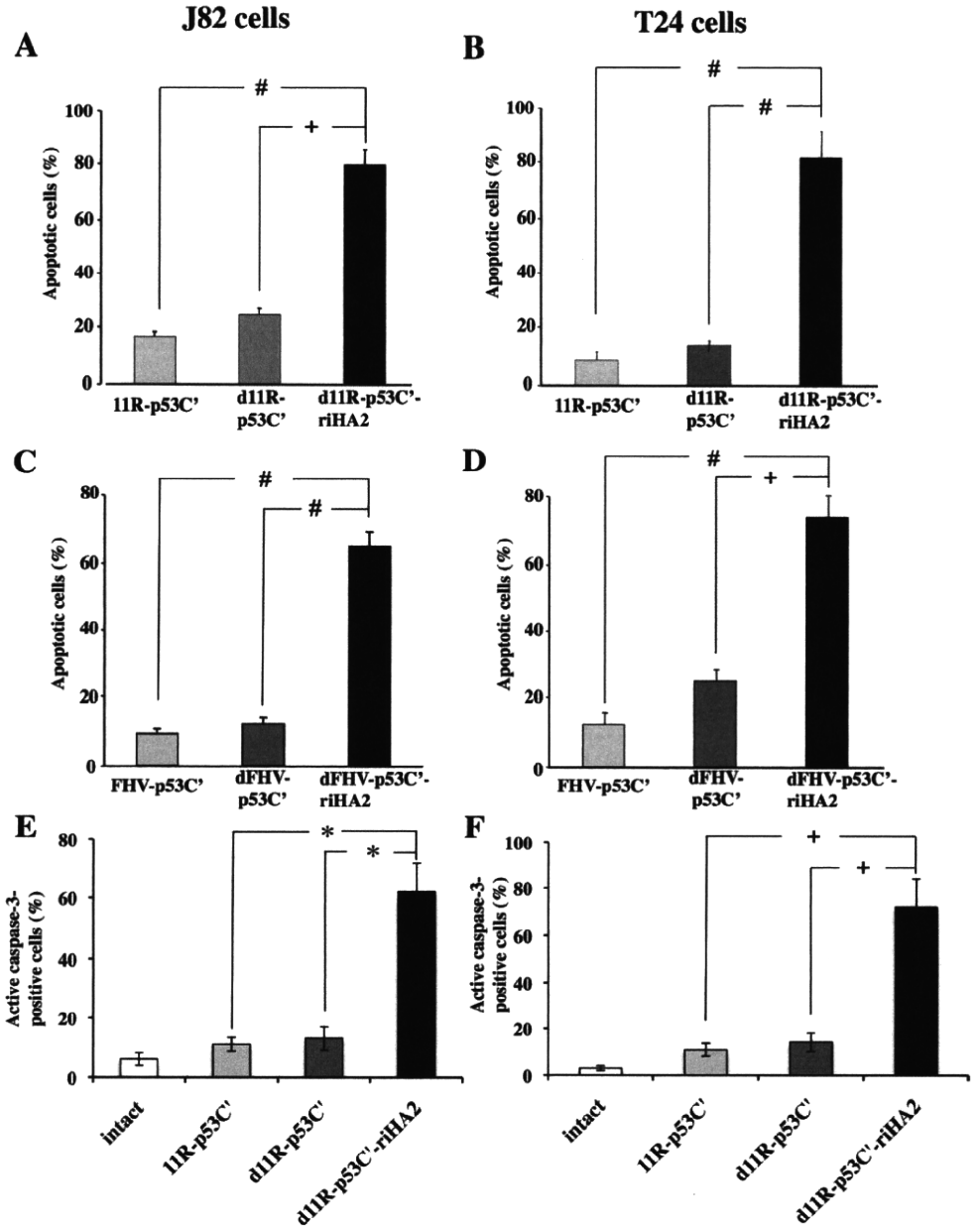

Figure 3. Effect of each CPP-fused p53C′ peptide on the induction of apoptosis and activation of caspase-3 in J82 and T24 cells. (A, B) Effect of 11R-p53C′, d11R-p53C′ and d11R-p53C′-riHA2 on the induction of apoptosis. (C and D) Effect of FHV-p53C′, dFHV-p53C′, and dFHV-p53C′-riHA2 on the induction of apoptosis. (E and F) Effect of 11R-p53C′, d11R-p53C′, and d11R-p53C′-riHA2 on the activation of caspase-3. (A, C, and E) J82 cells; (B, D, and F) T24 cells. Intact, no treatment with any peptide. n = 100 for each treatment. $^{+}P < .0005$, $^{\#}P < .0001$, and $^{*}P < .005$.

COMMENT

The present study has revealed the following 3 important findings. First, CPP-p53C′ did not inhibit the growth of bladder cancer cells with *p53* mutations. Second, the peptides connected with HA2 (d11R-p53C′-riHA2 and dFHV-p53C′-riHA2) significantly inhibited the growth of bladder cancer cells. Third, treatment with d11R-p53C′-riHA2 lengthened the survival of mice harboring peritoneal metastasis of bladder cancer.

In the advanced stage, bladder cancer is often resistant to chemotherapy and Bacillus Calmette-Guerin (BCG) therapy, and new strategies for treating the disease are clearly needed.[25] Gene therapy with the viral vector-mediated delivery of an anti-cancer gene such as *p53* may be an alternative treatment, and several preclinical studies of gene transfer by adenoviral vector into cancer cells in the bladder have been performed.[26–28] However, the efficiency of virus-mediated gene delivery is limited in bladder tumors.[29,30] In the present study, a D-isomer peptide of the p53 C-terminus connected with HA-2 or CPP (d11R-p53C′-riHA2 and dFHV-p53C′-riHA2) was effectively delivered into bladder cancer cells, and inhibited cell growth both in vitro and in vivo. The results suggest the transduction of cell-penetrating D-isomer peptides of the p53 C-terminus to be an attractive approach to the treatment of bladder cancer.

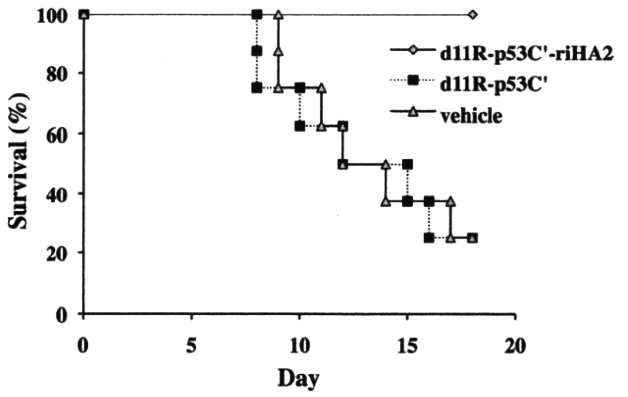

Figure 4. Effect of d11R-p53C′-riHA2 on survival rates of mice bearing peritoneal metastasis of bladder cancer. Mice were treated with d11R-p53C′-riHA2 and d11R-p53C′ at 20 mg/kg body weight or with PBS (vehicle) alone 3 days after the transplantation of tumor cells. The survival of the mice was measured by monitoring life span and data were analyzed using the Kaplan–Meier method.

Previous studies have shown that poly-arginine-fused p53 protein (11R-p53) inhibits the proliferation of human bladder and oral cancer cells as effectively as adenovirus-mediated p53 gene therapy, but with less cytotoxicity.[12,13] However, repeated administration of 11R-p53 is needed for transcriptional activation and the growth inhibition of cancer cells.[12] The transduced protein's entrapment in macropinosomes and rapid degradation may weaken its effect. In the present study, a single application of d11R-p53C′-riHA2 and dFHV-p53C′-riHA2 significantly inhibited the growth of bladder cancer in vivo, and a single application of d11R-p53C′-riHA2 increased long-term disease-free survival in vivo. The repeated application of proteins may evoke an immune response. Neither d11R-p53C′-riHA2 nor dFHV-p53C′-riHA2 caused problems associated with immunogenicity, suggesting that they would be effective against a significant proportion of bladder cancers.

A previous study showed that a transducible D-isomer p53 C-terminal peptide fused with TAT-PTD activated the p53 protein in cancer cells, and significantly increased lifespan in a preclinical model of terminal peritoneal carcinomatosis and peritoneal lymphoma.[21] However, the peptide was less effective against cancer cells expressing the mutant-type *p53* gene.[21] The results are consistent with the finding of the present study that TAT-p53C′ did not affect the growth of J82 and T24 cells expressing mutant p53. Moreover, neither d11R-p53C′ nor dFHV-p53C′ had an enough inhibitory effect on the growth of the bladder cancer cells. However, when attached to HA2, the peptides did inhibit the growth of such cells. HA-2 is a pH-sensitive fusogenic peptide that destabilizes lipid membranes at low pH and enhances the release of fusion proteins from macropinosomes.[14,15] When a poly arginine-fused p53 protein is linked to HA-2, it is released from macropinosomes of glioma cells and the anticancer effect is enhanced.[16] The molecular mechanism of the antitumor effect of HA-2–linked d11R-p53C′ on the growth of cancer cells expressing mutant p53 is unclear. Because CPPs-riHA2 (5 μM) had no cytotoxic effect on bladder cells, the p53C′ peptide essentially functions as an anti-cancer molecule. In bladder cancer cells expressing mutant *p53*, the CPP-fused p53C′ peptide may be entrapped in macropinosomes and HA-2 may be effective at releasing the peptide from macropinosomes. The mechanism involved is currently under investigation in our laboratory.

CONCLUSIONS

The present results showed that a single application of d11R-p53C′-riHA2 and dFHV-p53C′-riHA2 significantly inhibited the growth of bladder cancer cells. In a model of the peritoneal metastasis of bladder cancer, moreover, d11R-p53C′-riHA2 modulated tumor biology in vivo, resulting in a significant decrease in tumor burden, and an increase in lifespan and long-term disease-free survival. These results suggest that cell-penetrating D-isomer peptides of the p53 C-terminus with HA-2 may become a tool for bladder cancer therapy.

Acknowledgments. This work was supported by a Grant-in-aid for Scientific Research from the Ministry of Education, Science, Sports and Culture of Japan and by a Grant-in-aid for Scientific Research from the Ministry of Health, Labor and Welfare of Japan. Kentaro Takayama is grateful for JSPS Research Fellowship for Young Scientists.

References

1. Al-Sukhun S, Hussain M. Current understanding of the biology of advanced bladder cancer. Cancer. 2003;8:2064-2075.
2. Werthman PE, Drazan KE, Rosenthal JT, et al. Adenoviral-p53 gene transfer to orthotopic and peritoneal murine bladder cancer. J Urol. 1996;155:753-756.
3. Verma IM, Somia N. Gene therapy-promised, problems and prospects. Nature. 1997;389:239-242.
4. McCormick F. Cancer gene therapy: fringe or cutting edge. Nat Rev Cancer. 2001;1:130-141.
5. El-Andaloussi S, Holm T, Langel U. Cell-penetrating peptides: mechanisms and applications. Curr Pharm Des. 2005;11:3597-3611.
6. Gupta B, Levchenko TS, Torchilin VP. Intracellular delivery of large molecules and small particles by cell-penetrating proteins and peptides. Adv Drug Deliv Rev. 2005;57:637-651.
7. Wadia JS, Dowdy SF. Transmembrane delivery of protein and peptide drugs by TAT-mediated transduction in the treatment of cancer. Adv Drug Deliv Rev. 2005;57:579-596.
8. Futaki S, Suzuki T, Ohashi W, et al. Arginine-rich peptides: an abundant source of membrane-permeable peptides having potential as carriers for intracellular protein delivery. J Biol Chem. 2001;276:5836-5840.
9. Vives E, Brodin P, Lebleu B, et al. HIV-1 TAT protein basic domain rapidly translocates through the plasma membrane and accumulates in the cell nucleus. J Biol Chem. 1997;272:16010-16017.
10. Suzuki T, Futaki S, Niwa M, et al. Possible existence of common internalization mechanisms among arginine-rich peptides. J Biol Chem. 2002;277:2437-2443.
11. Wadia JS, Stan RV, Dowdy SF. Transducible TAT-HA fusogenic peptide enhances escape of TAT-fusion proteins after lipid raft macropinocytosis. Nat Med. 2004;10:310-315.

12. Takenobu T, Tomizawa K, Matsushita M, et al. Development of p53 protein transduction therapy using membrane-permeable peptides and the application to oral cancer cells. Mol Cancer Ther. 2002;1:1043-1049.
13. Inoue M, Tomizawa K, Matsushita M, et al. p53 protein transduction therapy: successful targeting and inhibition of the growth of the bladder cancer cells. Eur Urol. 2006;49:161-168.
14. Han X, Bushweller JH, Cafiso DS, et al. Membrane structure and fusion-triggering conformational change of the fusion domain from influenza hemagglutinin. Nat Struct Biol. 2001;8:715-720.
15. Skehel JJ, Cross K, Steinhauer D, et al. Influenza fusion peptides. Biochem Soc Trans. 2001;29:623-626.
16. Michiue H, Tomizawa K, Wei FY, et al. The NH_2 terminus of influenza virus hemagglutinin-2 subunit peptides enhances the antitumor potency of polyarginine-mediated p53 protein transduction. J Biol Chem. 2005;280:8285-8289.
17. Michael D, Oren M. The p53-Mdm2 module and the ubiquitin system. Semin Cancer Biol. 2003;13:49-58.
18. Bode AM, Dong Z. Post-translational modification of p53 in tumorigenesis. Nat Rev Cancer. 2004;4:793-805.
19. Olsson A, Manzl C, Strasser A, et al. How important are post-translational modifications in p53 for selectivity in target-gene transcription and tumour suppression? Cell Death Differ. 2007;14: 1561-1575.
20. Hupp TR, Sparks A, Lane DP. Small peptides activate the latent sequence-specific DNA binding function of p53. Cell. 1995;83: 237-245.
21. Snyder EL, Meade BR, Saenz CC, et al. Treatment of terminal peritoneal carcinomatosis by a transducible p53-activating peptide. PLoS Biol. 2004;2:186-193.
22. Futaki S, Kiwada T, Sugiura Y. Control of peptide structure and recognition by Fe(III)-induced helix destabilization. J Am Chem Soc. 2004;126:15762-15769.
23. Futaki S, Kitagawa K. Peptide-unit assembling using disulfide cross-linking: a new approach for construction of protein models. Tetrahedron Lett. 1994;35:1267-1270.
24. Wu HY, Tomizawa K, Oda Y, et al. Critical role of calpain-mediated cleavage of calcineurin in excitotoxic neurodegeneration. J Biol Chem. 2004;279:4929-4940.
25. Pfister C, Flaman JM, Dunet F, et al. p53 mutations in bladder tumors inactivate the transactivation of the p21 and Bax genes, and have a predictive value for the clinical outcome after bacillus Calmette-Guerin therapy. J Urol. 1999;162:69-73.
26. Werthman PE, Drazan KE, Rosenthal JT, et al. Adenoviral-p53 gene transfer to orthotopic and peritoneal murine bladder cancer. J Urol. 1996;155:753-756.
27. Chester JD, Kennedy W, Hall GD, et al. Adenovirus-mediated gene therapy for bladder cancer: efficient gene delivery to normal and malignant human urothelial cells in vitro and ex vivo. Gene Ther. 2003;10:172-179.
28. Siemens DR, Crist S, Austin JC, et al. Comparison of viral vectors: gene transfer efficiency and tissue specificity in a bladder cancer model. J Urol. 2003;170:979-984.
29. Li Y, Pong RC, Bergelson JM, et al. Loss of adenoviral receptor expression in human bladder cancer cells: a potential impact on the efficacy of gene therapy. Cancer Res. 1999;59:325-330.
30. Sachs MD, Rauen KA, Ramamurthy M, et al. Integrin alpha (v) and coxsackie adenovirus receptor expression in clinical bladder cancer. Urology. 2002;60:531-536.

Int. J. Radiat. Biol., Vol. 87, No. 3, March 2011, pp. 293–301

informa
healthcare

Induction of multinucleation in oral squamous cell carcinoma tissue with mutated p53 surviving boron neutron capture therapy

YUSEI FUJITA[1], NAOFUMI YAMAMOTO[1], ITSURO KATO[1], SOICHI IWAI[1], KOJI ONO[2], YOSHINORI SAKURAI[2], KEN OHNISHI[3], TAKEO OHNISHI[3], & YOSHIAKI YURA[1]

[1]*Department of Oral and Maxillofacial Surgery, Osaka University Graduate School of Dentistry, Osaka,* [2]*Particle Radiation Oncology Research Center Laboratory, Research Reactor Institute, Kyoto University, Osaka, and* [3]*Department of Biology, School of Medicine, Nara Medical University, Nara, Japan*

(Received 1 April 2010; Revised 10 September 2010; Accepted 29 September 2010)

Abstract

Purpose: To clarify the role of p53 in boron neutron capture therapy (BNCT) for oral squamous cell carcinoma (SCC), the effect of BNCT on oral SCC xenografts with either wild-type or mutant-type p53 was examined.

Materials and methods: Oral SCC cells expressing either wild-type (SAS/neo) or mutant-type p53 (SAS/mp53) were used to produce nude mouse tumours. Tumour-bearing mice received boronophenylalanine (BPA) at a dose of 250 mg/kg and tumours were exposed to neutron irradiation.

Results: After BNCT, the growth of SAS/neo and SAS/mp53 tumours was suppressed remarkably and all tumours became undetectable within two weeks. However, three of six SAS/mp53 tumours showed regrowth in two months. Histological examination of BNCT-treated tumours revealed chromosomal condensation, micronucleation, nuclear segmentation and intra- and intercelluar vacuolation. Notably, multinucleated giant cells appeared in SAS/mp53 tumours early after BNCT, suggesting mitotic catastrophe. In SAS/mp53 tumours treated with BNCT, a rapid decrease in phosphorylated cell division cycle 2 (cdc2) and a high level of cyclin B1, required for premature mitosis, were observed.

Conclusion: These results indicate that BNCT suppressed oral SCC xenografts in nude mice efficiently, but cells survived in mutant-type p53 tumours. BNCT induces multinucleation which represents prestage of apoptosis or necrosis in oral SCC with mutant-type p53, but it may be also associated with the recurrence of BNCT-treated tumours.

Keywords: *boron neutron capture therapy, p53, mitotic cell death, multinucleation, oral squamous cell carcinoma*

Introduction

The primary treatment of oral squamous cell carcinoma (SCC) consists of surgery and radiation therapy with or without chemotherapy, but there are a number of patients who show loco-regional recurrence (Wong et al. 2003, Palme et al. 2004). At more advanced stages, the radical removal of tumours results in severe deformities in the face and oral cavity. For patients whose cancers are considered inoperable and recur after primary therapy, new therapeutic strategies are required.

Boron neutron capture therapy (BNCT) is a binary system, involving the taking up of boron-10 (^{10}B)-enriched compounds by tumour cells and irradiation with thermal neutrons. ^{10}B absorbs a thermal neutron and yields an α(^{4}He) particle and a lithium (^{7}Li) nucleus, which have high linear energy transfer (LET) and path lengths in water of 5–10 μm. The success of BNCT is dependent on the selective uptake of sufficient amounts of ^{10}B into tumour cells as compared with surrounding normal tissues (Coderre and Morris 1999, Barth et al. 2005). BNCT has been demonstrated effective in the treatment of brain tumours, melanoma of the skin, metastatic liver tumours and locally advanced head and neck carcinomas (Fukuda et al. 2003, Kato et al. 2004, Kankaanranta et al. 2007, Miyatake et al. 2009, Zonta et al. 2009).

The cytotoxic effect of ionising radiation (IR) is mediated through pleiotropic mechanisms, which include interaction and damage of genomic DNA followed by activation of DNA damage-induced signaling pathways in a p53-dependent as well as

Correspondence: Dr Yoshiaki Yura, Department of Oral and Maxillofacial Surgery, Osaka University Graduate School of Dentistry, Osaka 565-0871, Japan. Tel: +81 6 6879 2941. Fax: +81 6 6879 2170. E-mail: yura@dent.osaka-u.ac.jp

ISSN 0955-3002 print/ISSN 1362-3095 online © 2011 Informa UK, Ltd.
DOI: 10.3109/09553002.2011.530336

p53-independent manner. These pathways culminate in cell cycle arrest and/or apoptosis, necrosis, autophagy or mitotic catastrophe (Debatin and Krammer 2004, Okada and Mak 2004).

Mitotic catastrophe, also known as mitotic death, has been widely described in cancer cells with mutant-type p53 in response to genotoxic damage and was initially characterised by chromosome missegregation followed by aberrant mitosis or imperfect cell division, leading to the formation of multinucleated cells (Erenpreisa and Cragg 2001). Most researchers considered that mitotic catastrophe represents a prestage of apoptosis or necrosis (Vakifahmetoglu et al. 2008). On the other hand, there is an opinion that it can be a mechanism of genotoxic resistance (Erenpreisa and Cragg 2001). Thus, mitotic catastrophe is controversial. Gamma ray irradiation, carbon-ion beams, iodine-131 and chemotherapeutic agents such as doxorubicin, cisplatin and paclitaxel have been shown to induce mitotic catastrophe (Ianzini et al. 2006, Vakifahmetoglu et al. 2008, Maalouf et al. 2009). With regard to BNCT, apoptosis has been detected in a small proportion of treated SCC cells (Masunaga et al. 2002, Kamida et al. 2006, Aromando et al. 2009), but other type of cell death such as mitotic catastrophe in response to BNCT has not. In the present study, we produced nude mouse tumours using oral SCC cells expressing wild- or mutant-type p53 with the same background and examined whether morphological alterations representing mitotic catastrophe can be induced by BNCT in a p53-independent manner. The results suggest that BNCT induces multinucleation in oral SCC with mutant-type p53, being accompanied by the recurrence of treated tumours.

Materials and methods

Cells

The oral SCC cell line SAS with the phenotype of wild-type p53 in IR-induced signal transduction was obtained from Japanese Collection of Research Bioresources (Tokyo, Japan). SAS cells were transfected with the plasmid pC53-248 containing an mp53 gene (codon 248, from Arg to Trp) to produce a dominant negative mp53 protein or with the control plasmid pCMV-Neo-Bam, which contains a neo-resistance marker. The stable transfectants SAS/mp53 and SAS/neo were used (Ota et al. 2000). These oral SCC cell lines were cultured in Dulbecco's modified Eagle's medium supplemented with 10% fetal bovine serum, 2 mM L-glutamine, 100 μg/ml penicillin, and 100 mg/ml streptomycin at 37°C in a humidified atmosphere with 5% CO_2.

Boron compounds and boron analysis

The boron compound boronophenylalanine (BPA) was purchased from Boron Biologicals, Inc. (Raleigh, NC, USA) and converted to a fructose complex to increase its solubility following the method reported by Coderre et al. (1994). The aqueous solution of BPA was prepared at a concentration of 250 mg/ml (21.28 mg ^{10}B/ml) and injected into mice carrying oral SCC intraperitoneally. Tumours and facial skin were sampled for ^{10}B measurements. Tissues were placed in Teflon tubes and ^{10}B concentrations were measured by prompt gamma-ray spectrometry using a thermal neutron guide installed at the Kyoto University Reactor (KUR) (Obayashi et al. 2004, Kamida et al. 2006). Six samples were used to determine the concentrations of ^{10}B.

BNCT for oral SCC xenografts in nude mice

To generate tumours, 1×10^6 SAS/neo or SAS/mp53 cells were inoculated subcutaneously into the back of the leg of 5-week-old female Balb/c nude mice (Clea Japan Inc., Tokyo, Japan). When the tumours were approximately 5 mm in diameter, the animals were used for experiments. The time from cell inoculation to BNCT was approximately 7 days in each group. Two hours after the intraperitoneal injection of BPA at a dose of 250 mg/kg, animals with either SAS/neo or SAS/mp53 tumours were given neutrons. Animals that received either SAS/neo or SAS/mp53 cells were also left untreated as a control.

Neutron irradiation was delivered via a neutron beam at 5 MW (thermal neutron mode 00-0011) in the KUR. During the irradiation for 70 min, the mouse was held stationary in a custom-designed acrylic resin box from which the tumour-bearing legs were pulled out through a narrow slit and fixed with adhesive. A LiF thermoplastic plate with a hole that defined the irradiation field was placed on the animal, so that only the tumour-bearing leg was exposed to the neutron beam. Neutron fluence was measured from the radioactivation of gold foil (3 mm in diameter, 0.05 mm thick) placed at the front and back of the tumours (Kamida et al. 2006). The average fluence of thermal neutrons was 8.19×10^{12} n/cm^2 and the average flux was 1.95×10^9 n/cm^2/s. Thermoluminescent dosimeters placed at the back of the tumours were used to measure contaminated γ-ray dosimetry and the dose of γ-rays was 1.41 Gy. The irradiation dose components were described previously (Kamida et al. 2008).The experiment was started at the time of neutron irradiation. Tumour length (L) and width (W) were measured every 3–4 days. Tumour volume (V) was determined by the formula: $V = LW^2/2$. Six tumours